SIAM J. SCI. COMPUT.
Vol. 37, No. 3, pp. A1525–A1553

RESIDUAL-BASED ADAPTIVITY AND PWDG METHODS FOR THE HELMHOLTZ EQUATION*

SHELVEAN KAPITA†, PETER MONK†, AND TIMOTHY WARBURTON‡

Abstract. We present a study of two residual a posteriori error indicators for the plane wave discontinuous Galerkin (PWDG) method for the Helmholtz equation. In particular, we study the h-version of PWDG in which the number of plane wave directions per element is kept fixed. First, we use a slight modification of the appropriate a priori analysis to determine a residual indicator. Numerical tests show that this is reliable but pessimistic in that the ratio between the true error and the indicator increases as the mesh is refined. We therefore introduce a new analysis based on the observation that sufficiently many plane waves can approximate piecewise linear functions as the mesh is refined. Numerical results demonstrate an improvement in the efficiency of the indicators.

Key words. PWDG, adaptivity, residual

AMS subject classifications. 65N30, 78M10, 35J20

DOI. 10.1137/140967696

1. Introduction.

We shall investigate the use of an adaptive plane wave discontinuous Galerkin (PWDG) method for approximating the solution of the Helmholtz equation with mixed boundary conditions. In particular, given a bounded Lipschitz polyhedral domain $\Omega \subset \mathbb{R}^2$ with boundary Γ consisting of two disjoint components Γ_D and Γ_A and unit outward normal ν, we want to approximate the solution u of

$$\Delta u + \kappa^2 u = 0 \quad \text{in } \Omega, \tag{1.1}$$

$$\frac{\partial u}{\partial \nu} + i\kappa u = g_A \quad \text{on } \Gamma_A, \tag{1.2}$$

$$u = 0 \quad \text{on } \Gamma_D. \tag{1.3}$$

Here, the wave number $\kappa > 0$ and $g_A \in L^2(\Gamma)$ is a given function. This problem is often considered because the Robin boundary condition (1.2) is a simple absorbing boundary condition, so the problem serves as a simplified model for scattering from a bounded domain. (In the scattering example, g_A is determined by the incident field.) In particular, we note that this problem is considered in [14], which has motivated part of our study. We could also include piecewise constant coefficients in the partial differential equation without any complication of the algorithm, but the proofs we shall present require constant coefficients.

The PWDG method we shall consider is a generalization of the ultra weak variational formulation (UWVF) of the Helmholtz equation due to Cessenat and Després [4, 5]. This method uses piecewise solutions of the Helmholtz equation in a nonstandard variational scheme on a finite element mesh to approximate the trace of u and the normal derivative of u on edges in the mesh. In [3], this was recognized to be

*Submitted to the journal's Methods and Algorithms for Scientific Computing section May 5, 2014; accepted for publication (in revised form) February 27, 2015; published electronically June 24, 2015.

http://www.siam.org/journals/sisc/37-3/96769.html

†Department of Mathematical Sciences, University of Delaware, Newark, DE 19716 (kapita@udel.edu, monk@math.udel.edu). The work of the authors was supported in part by NSF grant number DMS-1216620.

‡Computational and Applied Mathematics, Rice University, Houston, TX 77005–1892 (timwar@rice.edu). This author's work was supported in part by NSF grant DMS-1216674.

equivalent to a discontinuous Galerkin method, and this observation was then used to prove error estimates under restrictive conditions on the domain and mesh. At the same time, a generalized discontinuous Galerkin method based on possibly mesh dependent penalty parameters was analyzed using a classical approach in [10] and later using the approach of [3] in [11], where error estimates for a p-version exhibiting wave number dependence and a more precise estimate of approximation properties were calculated. In [13], exponential convergence of the hp PWDG method to smooth solutions is proved. Particularly important for this paper is the analysis in [14], where special penalty parameters are chosen that allow the derivation of an error estimate even on highly refined grids.

For background on PWDG and other methods using plane wave solutions for the Helmholtz equation, a useful paper is [7], and for a study of general DG methods for time harmonic wave propagation problems, see [19]. For computational aspects of PWDG, see [17], and for a dispersion analysis, see [9]. The UWVF or its PWDG generalization have been applied to Maxwell's equations [4, 15, 12], to the linear elastic Navier equation [16], and to the biharmonic problem [18].

We are interested in deriving a posteriori error indicators based on residuals to drive the PWDG method adaptively to a solution. To our knowledge, this is the first study of residual based adaptivity for these methods. Ideally, this study would include adaptivity in the number and direction of the basis functions per element (like p-adaptivity for polynomial methods) and also mesh refinement or h-adaptivity. Techniques for choosing the directions of plane-waves in the basis adaptively are investigated in [2, 1]. Related work, using ray tracing in the context of a conforming finite element method, can be found in [8]. We do not examine directional adaptivity here. Instead, we shall concentrate on more classical h-adaptivity, where we fix the number of basis functions per element and only refine the mesh.

We start from the observation that the estimates in [14] can easily be modified to give a residual based a posteriori error estimator for the L^2 norm. This is done in section 4. We then test these estimates on a model problem with a smooth solution. We find that the estimator is reliable but not efficient. It progressively overestimates the global L^2 norm error. Despite this, in the case of a smooth solution, the refinement path produces an optimal order approximation. A drawback of this type of adaptivity (i.e., reducing the mesh size for a constant number of directions per element) is that the conditioning of the linear system for the solution becomes very poor. Preliminary results in section 6.4 suggest that using a Bessel function basis helps in this regard.

It is clear from these numerical results (and the numerical experiments in [4]) that both the a priori and the a posteriori theory are not optimal with respect to the mesh width. We therefore revisit the derivation of the residual indicator. In particular, we note that from Lemma 3.10 in [10], on a refined mesh, sufficiently many plane wave basis functions can approximate piecewise linear finite element functions. This allows us to improve powers of the mesh size appearing in the a posteriori indicators. The theory behind this observation is presented in section 5. We then test the new indicators in section 6. The resulting residual estimators are seen to be an improvement over those in section 4. We then draw some conclusions and discuss possible extensions of this theory in section 7.

2. Notation and preliminaries. The domain $\Omega \subset \mathbb{R}^2$ for the problem is assumed to be Lipschitz smooth and to be an annular region in the sense that there are polygons Ω_A with boundary Γ_A and Ω_D with boundary Γ_D with connected boundaries such that the closure $\overline{\Omega}_D$ is strictly contained in Ω_A. We shall use the regularity

theory from [14, section 2] and so require that Ω_A is star-shaped with respect to the origin and Ω_D is star-shaped with respect to the open ball

$$B_{\gamma_R d_\Omega} = \{\mathbf{x} \mid |\mathbf{x}| < \gamma_R d_\Omega\}$$

for some $\gamma_R > 0$ and $d_\Omega = \operatorname{diam}(\Omega)$.

Using these domains,

$$\Omega = \Omega_A \setminus \overline{\Omega_D}.$$

To prove the existence of a solution to (1.1)–(1.3), the following space is used:

$$H^1_{\Gamma_D}(\Omega) = \left\{u \in H^1(\Omega) \mid u = 0 \text{ on } \Gamma_D\right\}.$$

The norm used is weighted with the wave-number:

$$\|u\|^2_{1,\kappa,\Omega} = \kappa^2 \|u\|^2_{L^2(\Omega)} + \|\nabla u\|^2_{L^2(\Omega)}.$$

Then it is shown in [14, Theorem 2.1] that there exists a weak solution to the abovementioned problem. In addition, if d_Ω is the diameter of Ω, then

$$\|u\|_{1,\kappa,\Omega} \leq C d_\Omega^{1/2} \|g_A\|_{L^2(\Gamma_A)}.$$

We assume that Ω is covered by a family of meshes $\mathcal{T}_h$ indexed by the maximum diameter of the elements in the mesh so that $h > 0$, and for any element $K \in \mathcal{T}_h$ we set

$$h_K = \operatorname{diam}(K),$$

where $\operatorname{diam}(K)$ is the diameter of the smallest circumscribed circle containing K.

Because we wish to derive a posteriori error indicators on refined meshes, we follow [14] and make the next three assumptions on the mesh:

Shape Regularity: For any element $K \in \mathcal{T}_h$, let ρ_K denote the diameter of the largest inscribed circle in K. Then there exists a constant μ independent of h such that for all K in $\mathcal{T}_h$, $h_K/\rho_K \leq \mu$.

Local quasi uniformity: Suppose $K_1, K_2 \in \mathcal{T}_h$ meet on an edge e. Then there exists a constant ζ independent of h such that

$$\zeta^{-1} \leq \frac{h_{K_1}}{h_{K_2}} \leq \zeta$$

for all such choices of K_1 and K_2.

Quasi uniformity close to Γ_A: There exists a constant τ_A such that for all h and all $K \in \mathcal{T}_h$ such that K shares an edge with Γ_A,

$$\frac{h}{h_K} \leq \tau_A.$$

As pointed out in [14], the goal is to refine the grid around the scatterer where the Dirichlet boundary condition occurs. The impedance boundary condition models an outgoing radiation condition, and so uniform refinement should occur near that boundary.

We make one other major assumption because we need to use results from [14] that depend on it: we assume that the triangles in the grid are all images of a finite

number of reference elements under dilation, translation, and rotation. This may be less of a concern for an adaptive method because the elements are obtained from a refinement of an initial coarse mesh, but in our numerical results we cannot ensure that this assumption holds.

Suppose that $K^{\pm}$ are a pair of elements sharing a common edge e and having outward normals $\nu^{\pm}$, respectively. We define the jumps and averages of a suitably smooth function $v^{\pm}$ defined on each element by

$$\{\!\{v\}\!\} = \frac{1}{2}(v^+ + v^-)|_e, \qquad [\![v]\!] = (v^+\nu^+ + v^-\nu^-)|_e.$$

Similarly, for a piecewise defined vector function $\mathbf{v}^{\pm}$ we define

$$\{\!\{\mathbf{v}\}\!\} = \frac{1}{2}(\mathbf{v}^+ + \mathbf{v}^-)|_e, \qquad [\![\mathbf{v}]\!] = (\mathbf{v}^+ \cdot \nu^+ + \mathbf{v}^- \cdot \nu^-)|_e.$$

The set of interior edges of elements in $\mathcal{T}_h$ is denoted $\mathcal{E}_I$. Edges on the boundary Γ_A are denoted $\mathcal{E}_A$ and on Γ_D by $\mathcal{E}_D$. In later sections, we shall make frequent use of the following trace inequality: for any edge e of a triangle K and any $w \in H^1(K)$, there exists a constant C independent of K and w such that

$$\|w\|^2_{L^2(e)} \le C\left(\frac{1}{h_K}\|w\|^2_{L^2(K)} + h_K\|\nabla w\|^2_{L^2(K)}\right). \tag{2.1}$$

In addition, under the assumptions on the mesh (in particular that all elements are the affine image of a finite number of reference elements), estimate (24) of [14] states that if $w \in H^{s+3/2}(K)$ for some $1/2 \ge s > 0$, then

$$\|\nabla w\|_{L^2(e)} \le C\left(h_K^{-1}\|\nabla w\|^2_{L^2(K)} + h_K^{2s}|\nabla w|^2_{H^{1/2+s}(K)}\right), \tag{2.2}$$

where $|\cdot|_{H^{1/2+s}(K)}$ is the $H^{1/2+s}(K)$ seminorm.

The PWDG method used here is based on the use of plane waves propagating in different directions on each element. Let p_K denote the number of directions used on element K, and this will be fixed in this paper. We use uniformly spaced directions on the unit circle

$$\mathbf{d}_j^K = (\cos(\theta_j^K), \sin(\theta_j^K)),\ 1 \le j \le p_K,$$

where $\theta_j^K = 2\pi j/p_K$. On an element K, the local solution space is

$$V_{P_K}^K = \operatorname{span}\left\{\exp(ik\mathbf{d}_j^K \cdot \mathbf{x}), \quad 1 \le j \le p_K\right\}.$$

Then the global solution space is

$$V_h = \left\{u_h \in L^2(\Omega) \mid u_h|_K \in V_{p_K}^K\ \forall K \in \mathcal{T}_h\right\}. \tag{2.3}$$

3. The PWDG method. Since our code is based on the discontinuous Galerkin approach to discretizing first order systems, we give a very brief derivation of PWDG. This derivation can also be found in [14]. (See also [3] for connection to the UWVF method.) We start by introducing a vector variable σ such that

$$i\kappa\sigma = \nabla u, \text{ so } i\kappa u = \nabla \cdot \sigma.$$

Multiplying these equations by the complex conjugate of smooth test functions v and τ, integrating over an element K, and adding the results, we obtain

$$\int_K \{i\kappa\sigma\cdot\overline{\tau}+u\nabla\cdot\overline{\tau}+i\kappa u\overline{v}+\sigma\cdot\nabla\overline{v}\}\,dA=\int_{\partial K}\{u\overline{\tau\cdot\nu}+\sigma\cdot\nu\overline{v}\}\,ds.$$

Rearranging and replacing the boundary flux terms $(u,\sigma\cdot\nu)$ on the right-hand side by consistent numerical fluxes $(\hat{u},\hat{\sigma}\cdot\nu)$ (we will specify the fluxes shortly), we obtain

$$\int_K \left\{\sigma\cdot(\overline{-i\kappa\tau+\nabla v})+u(\overline{-i\kappa v+\nabla\cdot\tau})\right\}\,dA=\int_{\partial K}\{\hat{u}\overline{\tau\cdot\nu}+\hat{\sigma}\cdot\nu\overline{v}\}\,ds.$$

Finally, assuming the test functions also satisfy the first order system corresponding to the Helmholtz equation,

$$i\kappa\tau=\nabla v,\ \text{so}\ i\kappa v=\nabla\cdot\tau,$$

we obtain

$$\int_{\partial K}\{\hat{u}\overline{\tau\cdot\nu}+\hat{\sigma}\cdot\nu\overline{v}\}\,ds=0 \tag{3.1}$$

on each element in the mesh.

It remains to detail the fluxes. We follow [14]. On an interior edge in the mesh, we take the numerical fluxes to be

$$\begin{aligned}\hat{u}&=\{\!\{u\}\!\}-\frac{\beta}{\mathrm{i}\kappa}[\![\nabla_h u]\!],\\ ik\widehat{\sigma}&=\{\!\{\nabla_h u\}\!\}-\mathrm{i}\kappa\alpha[\![u]\!].\end{aligned}$$

Here, $\nabla_h u$ is the broken (piecewise) gradient. On boundary edges on Γ_A, the fluxes are

$$\begin{aligned}\hat{u}&=u-\delta((i\kappa)^{-1}\nabla_h u\cdot\nu+u-(i\kappa)^{-1}g_A),\\ i\kappa\widehat{\sigma}&=\nabla_h u-(1-\delta)(\nabla_h u+i\kappa u\nu-g_A\nu).\end{aligned}$$

Finally, on edges on the Dirichlet portion of the boundary, the fluxes are

$$\begin{aligned}\hat{u}&=0,\\ i\kappa\widehat{\sigma}&=\nabla_h u-\alpha i\kappa u\nu.\end{aligned}$$

Adding (3.1) over all elements in the mesh and using the above fluxes, we obtain the PWDG method of [14] (with appropriate sign changes to allow for our exterior boundary condition). In particular, let

$$\begin{aligned}A_h(u,v)=&\int_{\mathcal{E}_I}\{\!\{u\}\!\}[\![\nabla_h\overline{v}]\!]\,ds-\int_{\mathcal{E}_A}\delta(\nabla_h u\cdot\nu)\overline{v}\,ds-\int_{\mathcal{E}_I}[\![\overline{v}]\!]\cdot\{\!\{\nabla_h u\}\!\}\,ds\\&+\int_{\mathcal{E}_A}(1-\delta)u(\nu\cdot\nabla_h\overline{v})\,ds-\frac{1}{i\kappa}\int_{\mathcal{E}_I}\beta[\![\nabla_h u]\!][\![\nabla_h\overline{v}]\!]\,ds\\&-\frac{1}{i\kappa}\int_{\mathcal{E}_A}\delta(\nu\cdot\nabla_h u)(\nu\cdot\nabla_h\overline{v})\,ds+i\kappa\int_{\mathcal{E}_I}\alpha[\![u]\!]\cdot[\![\overline{v}]\!]\,ds\\&+i\kappa\int_{\mathcal{E}_A}(1-\delta)u\overline{v}\,ds-\int_{\mathcal{E}_D}(\nabla_h u\cdot\nu)\overline{v}\,ds+\int_{\mathcal{E}_D}\alpha i\kappa u\overline{v}\,ds\end{aligned} \tag{3.2}$$

and

$$\ell(v) = -\frac{1}{i\kappa}\int_{\mathcal{E}_A} \delta g_A(\nu\cdot\nabla_h\overline{v})\,ds + \int_{\mathcal{E}_A}(1-\delta)g_A\overline{v}\,ds. \tag{3.3}$$

An important contribution of [14] is that on a refined mesh, the coefficients can be chosen as follows. Let e be an edge in the mesh having length h_e, and then

$$\alpha|_e = \frac{ah}{h_e},\ \beta|_e = \frac{bh}{h_e},\ \delta|_e = \frac{dh}{h_e} \le \frac{1}{2}, \tag{3.4}$$

where a, b, d are positive constants. A contribution from this paper is to also analyze the choice of mesh independent parameters. Then the discrete solution $u_h \in V_h$ satisfies

$$A_h(u_h, v) = \ell(v) \qquad \forall v \in V_h.$$

In [14], it is shown that this equation has a solution regardless of the mesh size and wave number, and a global $L^2(\Omega)$ norm error estimate is proved. Therefore, we shall concentrate on a posteriori estimates for the global L^2 norm here. Version (3.2) of the method is convenient for programming but not for a posteriori analysis due to the presence of averages of the unknown field.

We now recall an equivalent form of the sesquilinear form $A_h(\cdot,\cdot)$ based on using the following "magic lemma."

LEMMA 3.1 (Lemma 6.1 from [7]). *For any sufficiently smooth piecewise defined vector field σ and piecewise defined function v,*

$$\sum_{K\in T_h}\int_{\partial K}\sigma\cdot n\overline{v}\,ds = \int_{\mathcal{E}_\mathcal{I}}[\![\overline{v}]\!]\cdot\{\!\{\sigma\}\!\}\,ds + \int_{\mathcal{E}_\mathcal{I}}\{\!\{\overline{v}\}\!\}\cdot[\![\sigma]\!]\,ds + \int_{\mathcal{E}_\mathcal{A}\cup\mathcal{E}_\mathcal{D}}\overline{v}\nu\cdot\sigma\,ds.$$

Using this lemma to rewrite appropriate terms in (3.2) and using the identity that

$$0 = \int_K(-\Delta u - k^2u)\overline{v}\,dA = \int_K(\nabla u\cdot\nabla\overline{v} - k^2u\overline{v})\,dA - \int_{\partial K}\frac{\partial u}{\partial\nu}\overline{v}\,ds,$$

we obtain, for any pair of piecewise solutions of the Helmholtz equation (u, v), respectively, in $H^{3/2+s}(K)$, $s > 0$,

$$\begin{aligned} A_h(u,v) = {} & \int_\Omega\left(\nabla_h u\cdot\nabla_h\overline{v} - \kappa^2 u\,\overline{v}\right)dA - \int_{\mathcal{E}_\mathcal{I}}\left(\{\!\{\nabla_h u\}\!\}\cdot[\![\overline{v}]\!] + [\![u]\!]\cdot\{\!\{\nabla_h\overline{v}\}\!\}\right)ds \\ & - \frac{1}{i\kappa}\int_{\mathcal{E}_\mathcal{I}}\beta\,[\![\nabla_h u]\!]\,[\![\nabla_h\overline{v}]\!]\,ds + i\kappa\int_{\mathcal{E}_\mathcal{I}}\alpha\,[\![u]\!]\cdot[\![\overline{v}]\!]\,ds - \int_{\mathcal{E}_\mathcal{A}}\delta u\nabla_h\overline{v}\cdot\nu\,ds \\ & - \int_{\mathcal{E}_\mathcal{A}}\delta\nabla_h u\cdot\nu\overline{v}\,ds - \frac{1}{i\kappa}\int_{\mathcal{E}_\mathcal{A}}\delta(\nabla_h u\cdot\nu)(\nabla_h\overline{v}\cdot\nu)\,ds + i\kappa\int_{\mathcal{E}_\mathcal{D}}\alpha u\overline{v}\,ds \\ & + i\kappa\int_{\mathcal{E}_\mathcal{A}}(1-\delta)u\overline{v}\,ds - \int_{\mathcal{E}_\mathcal{D}}\left((\nabla_h u\cdot\nu)\overline{v} + u(\nabla_h\overline{v}\cdot\nu)\right)ds. \end{aligned} \tag{3.5}$$

This form, although useful for proving DG coercivity, is still not the most convenient for a posteriori analysis for the same reason as before. Integrating the first term by parts again, using the magic lemma, and recalling also that u satisfies the Helmholtz

equation on each element, we obtain

$$
\begin{aligned}
(3.6)\quad A_h(u,v) = &\int_{\mathcal{E}_\mathcal{I}} (\llbracket \nabla_h u \rrbracket \{\!\{\overline{v}\}\!\} - \llbracket u \rrbracket \cdot \{\!\{\nabla_h \overline{v}\}\!\})\, ds - \frac{1}{i\kappa}\int_{\mathcal{E}_\mathcal{I}} \beta \llbracket \nabla_h u \rrbracket \llbracket \nabla_h \overline{v} \rrbracket\, ds \\
&+ i\kappa \int_{\mathcal{E}_\mathcal{I}} \alpha \llbracket u \rrbracket \cdot \llbracket \overline{v} \rrbracket\, ds - \int_{\mathcal{E}_\mathcal{A}} \frac{\delta}{i\kappa}(i\kappa u + \nabla_h u \cdot \nu)\nabla_h \overline{v} \cdot \nu\, ds \\
&+ \int_{\mathcal{E}_\mathcal{A}} (1-\delta)(\nabla_h u \cdot \nu + i\kappa u)\overline{v}\, ds + \int_{\mathcal{E}_\mathcal{D}} u(i\kappa\alpha\overline{v} - \nabla_h \overline{v} \cdot \nu)\, ds.
\end{aligned}
$$

Comparing (3.6) and (3.2), we see that (3.6) now involves residuals of u on the boundary that arise in estimating how well the boundary conditions are satisfied and does not involve averages of u.

4. A posteriori estimates I. In this section we shall prove an a posteriori error estimate using residuals in the global L^2 norm. This is the theoretical basis for the ESTIMATE step in the adaptive cycle of our code.

We shall need the solution of the following adjoint problem of finding $z \in H^1(\Omega)$ such that

$$
-\Delta z - \kappa^2 z = (u - u_h) \text{ in } \Omega, \tag{4.1}
$$

$$
\frac{\partial z}{\partial \nu} - i\kappa z = 0 \text{ on } \Gamma_A, \tag{4.2}
$$

$$
z = 0 \text{ on } \Gamma_D. \tag{4.3}
$$

Theorem 3.2 of [14] shows that a unique solution exists for the above problem and $z \in H^{3/2+s}(\Omega)$ for some $1/2 \geq s > 0$ (determined by the reentrant angles of the boundary). In addition

$$
\sqrt{\|\nabla z\|^2_{L^2(\Omega)} + \kappa^2 \|z\|^2_{L^2(\Omega)}} \leq C d_\Omega \|u - u_h\|_{L^2(\Omega)}, \tag{4.4}
$$

$$
|\nabla z|_{H^{1/2+s}(\Omega)} \leq C(1 + d_\Omega \kappa) d_\Omega^{1/2-s} \|u - u_h\|_{L^2(\Omega)}, \tag{4.5}
$$

where d_Ω is the diameter of Ω. Furthermore, the following bound is proved before equation (21) in [13]. There is a constant C depending only on the shape of the domain such that

$$
\|z\|^2_{L^\infty(\Omega)} \leq C \frac{d_\Omega^2}{\text{area}(\Omega)} (\kappa^{-2} + d_\Omega^4 \kappa^2) \|u - u_h\|^2_{L^2(\Omega)}. \tag{4.6}
$$

The following theorem provides an estimate of the global L^2 error in terms of computable quantities (and an overall scaling constant). It does not use any special properties of the PWDG solution and is applicable, for example, to the least squares solution.

THEOREM 4.1. *Let $u_h \in V_h$, and then there exists a constant C depending only on μ, s, γ_R and the flux parameters a, b, d, but independent of h, p, κ, u, u_h such that*

$$
\|u - u_h\|_{L^2(\Omega)} \leq C \zeta^{1/2} d_\Omega \left[1 + (d_\Omega \kappa)^{1/2} (d_\Omega^{-1} h)^s (\kappa h)^{1/2}\right] \eta_{DG}(u_h), \tag{4.7}
$$

where s is the regularity exponent in (4.5) *and the residual error indicator is given by*

$$
\begin{aligned}
(4.8)\quad \eta_{DG}(u_h)^2 = (\kappa h)^{-1} \Big(&\kappa^{-1} \|\beta^{1/2} \llbracket \nabla_h u_h \rrbracket\|^2_{L^2(\mathcal{E}_I)} + \kappa \|\alpha^{1/2} \llbracket u_h \rrbracket\|^2_{L^2(\mathcal{E}_I)} \\
&+ \kappa^{-1} \|\delta^{1/2}(g - \nabla u_h \cdot \nu - i\kappa u_h)\|^2_{L^2(\Gamma_A)} + \kappa \|\alpha^{1/2} u_h\|^2_{L^2(\Gamma_D)} \Big).
\end{aligned}
$$

Remark. Clearly, the overall constant multiplying $\eta_{DG}(u_h)$ in Theorem 4.1 blows up as κ increases at fixed h. The coarse initial mesh needs to be fine enough to provide some approximation to the true field.

Proof. The proof of this theorem follows closely the proof of [14, Lemma 4.4] (also [11, Lemma 3.7]), so we only give sufficient detail to observe the changes. Let $w = u - u_h$, then using the adjoint problem (4.1) and integrating by parts on each element K, followed by the fact that w is a piecewise solution of the Helmholtz equation, together with the boundary conditions on z, we get

$$\begin{aligned}\int_\Omega |w|^2\,dA &= \sum_{K\in\mathcal{T}_h}\int_{\partial K}\left(\frac{\partial w}{\partial\nu}\overline{z} - w\frac{\partial\overline{z}}{\partial\nu}\right)\,ds\\ &= \int_{\mathcal{E}_\mathcal{I}}\left(\llbracket\nabla_h w\rrbracket\,\overline{z} - \llbracket w\rrbracket\cdot\nabla_h\overline{z}\right)\,ds\\ &\quad + \int_{\mathcal{E}_\mathcal{A}}\left(\nabla_h w\cdot\nu + i\kappa w\right)\overline{z}\,ds - \int_{\mathcal{E}_\mathcal{D}} w\nabla_h\overline{z}\cdot\nu\,ds.\end{aligned}$$

The only difference with the results in [14] is to retain the boundary condition for w so that it generates a residual in the final estimate. Indeed, the Cauchy–Schwarz inequality, together with the equation and transmission or boundary conditions for u, then gives

$$\|u-u_h\|^2_{0,\Omega} \le \eta_{DG}(u_h)(\kappa h)^{1/2}\mathcal{G}(z)^{1/2}, \tag{4.9}$$

where

$$\begin{aligned}\mathcal{G}(z) := &\sum_{e\in\mathcal{E}_\mathcal{I}}\left(\kappa\|\beta^{-1/2}z\|^2_{L^2(e)} + \kappa^{-1}\|\alpha^{-1/2}\nabla_h z\cdot\nu\|^2_{L^2(e)}\right)\\ &+\sum_{e\in\mathcal{E}_\mathcal{A}}\kappa\|\delta^{-1/2}z\|^2_{L^2(e)} + \sum_{e\in\mathcal{E}_\mathcal{D}}\kappa^{-1}\|\alpha^{-1/2}\nabla_h z\cdot\nu\|^2_{L^2(e)}.\end{aligned}$$

Proceeding to estimate $(\kappa h)^{1/2}\mathcal{G}(z)$ as in [14, Lemma 4.4] gives the theorem. ∎

We now test the error indicators derived above to drive h-adaptivity. (We keep the number of directions per element fixed and equal on all elements.) Our first test uses a smooth solution on an L-shaped domain. In this case, uniform refinement is likely to be optimal, and we expect the adaptive method to result in an approximately uniform mesh. All computations are done in MATLAB, and we shall discuss the algorithm later in section 6.

We consider an L-shaped domain $\Omega = (-1,1)^2\backslash([0,1]\times[-1,0])$. We choose Dirichlet boundary conditions such that the exact solution of (1.1) is given by

$$u(\mathbf{x}) = J_\xi(\kappa r)\sin(\xi\theta), \tag{4.10}$$

where $\mathbf{x} = r(\cos\theta,\sin\theta)$ for $\xi = 2$ (later we will also choose $\xi = 2/3$ corresponding to a singular solution) and $\kappa = 12$. Here, J_ξ denotes the Bessel function of the first kind and order ξ. The solution is shown in Figure 1. Note that although we have not implemented the impedance boundary condition, the theory in this section can also be proved with just the Dirichlet boundary condition provided κ^2 is not an interior Dirichlet eigenvalue for the domain. In the Dirichlet case, the dependence of the overall coefficient on κ cannot be estimated. But the overall constant is not used in the marking strategy.

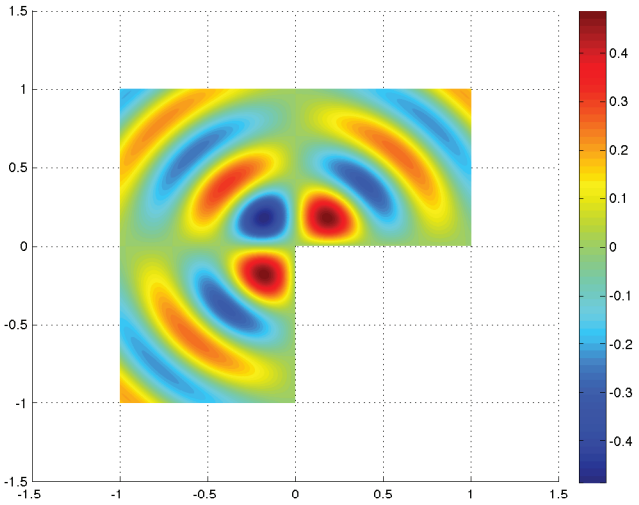

FIG. 1. *The computed solution after* 12 *iterations when* $\xi = 2$ *and* $k = 12$ *using* $p_K = 7$ *plane waves per element. This is indistinguishable graphically from the exact solution.*

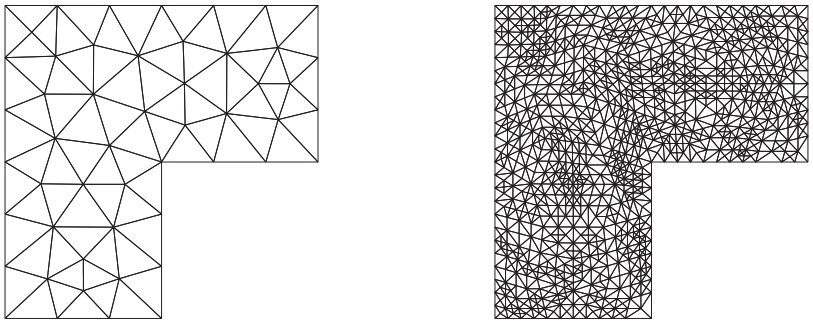

(a) Initial (b) After 12 iterations

FIG. 2. *The left panel shows the initial mesh, and the right panel shows the adaptively computed mesh after* 12 *iterations when* $\xi = 2$ *and* $k = 12$ *using* $p_K = 7$ *plane waves per element.*

The initial mesh and the refined mesh after 12 adaptive steps are shown in Figure 2. We see that the adaptive scheme has correctly chosen to refine almost uniformly in the domain since there is no singularity at the reentrant corner.

In Figure 3, we show detailed error results starting from the mesh in Figure 2 using the indicator in Theorem 4.1 with $p_K = 5$ plane waves per element. The code uses the Doerfler marking strategy with a bulk parameter $\theta = 0.3$. (See the discussion in section 6.) In these figures, we show the relative error in L^2 norm and the indicator η_{DG}. We scale the indicator so that the indicator and actual relative error are equal at the first step. For reliability, we then want the estimated error to lie above the true error, and for efficiency we want the gap between the two curves to be small. Of course, until the mesh is refined sufficiently, both efficiency and reliability may not be observed. In the right panel of each figure, we show the ratio of the exact relative error to the error indicator and term this the "efficiency ratio." The efficiency decreases markedly as the algorithm progresses.

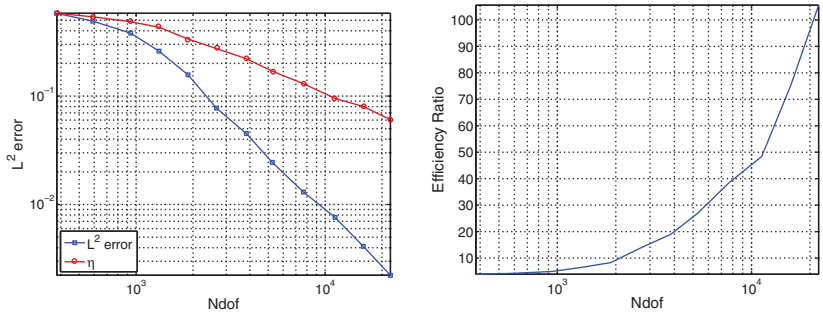

FIG. 3. *Adaptive refinement using $p_K = 5$ waves per element and the indicator from Theorem* 4.1. *Left panel: relative L^2 norm and indicator. Right panel: efficiency in the L^2 norm. Although the indicator is reliable, it tends to overestimate the error, so is not efficient.*

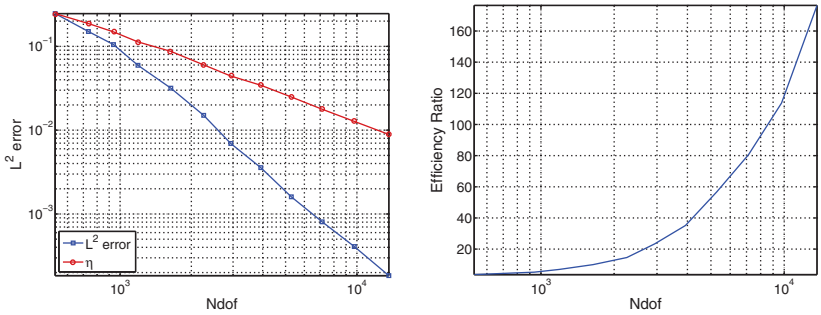

FIG. 4. *Adaptive refinement using $p_K = 7$ waves per element and the indicator from Theorem* 4.1. *Left panel: relative L^2 norm behavior. Right panel: efficiency in the L^2 The behavior of the indicator is similar to that for $p_K = 5$ in Figure* 3.

Results for $p^K = 7$ waves per element are shown in Figure 4. Again, mesh refinement does improve the solution error, but the efficiency of the indicator deteriorates rapidly as the mesh is refined.

5. A posteriori estimates II. The results at the end of section 4 show that the basic error indicator in Theorem 4.1, while reliable, is not efficient. We therefore need to reexamine h-convergence theory to determine if a different weighting for the residual can be derived.

In section 4 we used special weights α and β designed to allow the estimation of $\mathcal{G}(z)$ in terms of inverse powers of the global mesh size. Because of the upcoming results in this section, we no longer need inverse powers of the global mesh size in the estimate, and we now make the choice that the parameters α, β, and δ are positive constants independent of the mesh size and that $\delta < 1$. Note that the choice $\alpha = \beta = \delta = 1/2$ gives the classical UWVF [3]. We want an a posteriori error estimate for $\|u - u_h\|_{L^2(\Omega)}$ and will again use the solution z of the adjoint problem (4.1)–(4.3). By the adjoint consistency of the PWDG method (or direct calculation), we see that z is sufficiently smooth to satisfy

$$A_h(w, z) = \int_\Omega w(\overline{u - u_h})\, dA$$

for all sufficiently smooth piecewise solutions w of the Helmholtz equation. ($w \in H^{3/2+s}(K)$ for some $s > 0$ on each element suffices.)

The techniques we use to derive our a posteriori estimates are related to those in [10] in that we use the fact that plane waves can approximate piecewise linear functions. Since $z \in H^{3/2+s}(\Omega)$, $s > 0$, we can interpolate z by a standard piecewise linear finite element function denoted z_h^c. We shall need to approximate z_h^c by a function $z_{pw,h}$. That this is possible follows from the proof of Lemma 3.10 in [10] and is given in Lemma 6.3 in [13]. We give a slightly modified version.

LEMMA 5.1. *Suppose that on an element K we are using $P_K \geq 4$ plane waves denoted $\{\psi_j^K\}_{j=1}^{P_K}$. Then there are constants $\{\alpha_{i,j}^K\}$ (depending on κ) for $0 \leq i \leq 2$ and $1 \leq j \leq P_K$ such that if $\mu_{pw}^i = \sum_{j=1}^{P_K} \alpha_{i,j}^K \psi_j^K$ and for all $x = (x_1, x_2) \in K$*

$$\begin{aligned} |1 - \mu_{pw}^0| &= O(\kappa^2|x|^2), & |\nabla \mu_{pw}^0| &= O(\kappa^2|x|), \\ |x_j - \mu_{pw}^j| &= O(\kappa^2|x|^3), & |\nabla(x_j - \mu_{pw}^j)| &= O(\kappa^2|x|^2),\ j = 1, 2, \\ |\nabla\nabla \mu_{pw}^0| &= O(\kappa^2), & |\nabla\nabla \mu_{pw}^j| &= O(\kappa^2|x|),\ j = 1, 2, \end{aligned}$$

as $|x| \to 0$.

Remark 1. This lemma is motivated by the following observation. Suppose we are in one dimension and on the interval $[-h/2, h/2]$. Let the basis functions be $\psi_1(x) = \exp(i\kappa x)$ and $\psi_2(x) = \exp(-i\kappa x)$. Then

$$\begin{aligned} \mu^0(x) &= \frac{\psi_1(x) + \psi_2(x)}{2} = \cos(\kappa x) = 1 - O(\kappa^2 x^2), \\ \mu^1(x) &= \frac{\psi_1(x) - \psi_2(x)}{2i\kappa} = \frac{\sin(\kappa x)}{\kappa} = x - O(\kappa^2 x^3) \end{aligned}$$

give a good approximation to linear functions for small h. Other estimates follow accordingly.

If we select $p_K = 3$ waves per element

$$\psi_j(x, y) = \exp(i\kappa(\cos(\theta_j)x_1 + \sin(\theta_j)x_2)), \quad j = 1, 2, 3,$$

where $\theta_j = (2\pi/3)(j-1)$, then we can compute coefficients $\alpha_{i,j}$ such that

$$\begin{aligned} \mu_{pw}^0 &= 1 + O(|x|^2\kappa^2), \\ \mu_{pw}^j &= x_j + O(|x|^2\kappa), \end{aligned}$$

provided $-\sin(\theta_2) + \sin(\theta_3) - \cos(\theta_2)\ \sin(\theta 3) + \sin(\theta_2)\ \cos(\theta_3) \neq 0$. But equality only occurs if $\theta_2 = 0$ or $\theta_2 = \theta_3$, so this condition is satisfied. These results are not sufficient for the lemma but could be used to derive an alternative indicator in this case.

If we choose $p_K = 4$, we have

$$\psi_1 = \exp(i\kappa x_1),\ \psi_2(x) = \exp(i\kappa x_2),\ \psi_3(x) = \exp(-i\kappa x_1),\ \psi_4(x) = \exp(-i\kappa x_2).$$

Then Lemma 5.1 is satisfied because the approximation problem reduces to the one-dimensional case.

When $p_K = 5$ with equally spaced directions, a symbolic algebra package (Maple) again verifies the required asymptotics. Indeed, this is the lowest order case considered in [10, 13], where a general proof is given for $p_K \geq 5$.

Now suppose we are on a triangle K and $z_h^c = \sum_{j=1}^3 z(\mathbf{a}_j^K)\lambda_j^K$, where λ_j^K is the jth barycentric coordinate function and $\mathbf{a}_j^K$ is the jth vertex of the triangle. We can

assume that the centroid is at the origin by translation. Then, $\lambda_j^K = a_j^K + b_j^K x_1 + c_j^K x_2$ and $a_j^K = O(1)$, $b_j^K = O(1/h_K)$ and $c_j^K = O(1/h_K)$. Replacing 1, x_1, and x_2 by the above plane wave approximations μ_{pw}^j, $j = 0, 1, 2$, and denoting this approximation by $\lambda_{pw,j}^K$, we have the following.

LEMMA 5.2. *For $p_K \geq 4$, we have the following estimates for all $x \in K$,*

$$|\lambda_j^K - \lambda_{pw,j}^K| + h_K|\nabla(\lambda_j^K - \lambda_{pw,j}^K)| + h_K^2|\nabla\nabla(\lambda_j^K - \lambda_{pw,j}^K)| \leq C(h_K^2\kappa^2).$$

Remark 2. This lemma is essentially used in the proof of Lemma 3.10 in [10].

Proof. To estimate $\lambda_j^K - \lambda_{pw,j}^K$ on K, we note that

$$\begin{aligned}|\lambda_j^K - \lambda_{pw,j}^K| &= |a_j^K(1 - \mu_{pw}^0) + b_j^K(x_1 - \mu_{pw}^1) + c_j^K(x_2 - \mu_{pw}^2)| \\ &\leq C(k^2|x|^2 + (1/h_K)(k^2h_K^3)) \leq C\kappa^2h_K^2.\end{aligned}$$

The proof of the other estimates proceeds similarly. ∎

Using the plane wave approximation to the barycentric coordinate functions element by element, we can then construct an approximate interpolant $z_{pw,h} \in V_h$. We need to estimate $z_h^c - z_{pw,h}^c$ and $\nabla_h(z_h^c - z_{pw,h})$ on edges in the mesh. This is done in the next lemma

LEMMA 5.3. *Suppose e is an edge between two elements K_1 and K_2. Under the standing assumptions on the mesh, there is a constant C independent of e, z, K_j, h_{K_j}, $j = 1, 2$, and κ such that*

$$\| \{\!\{ z_h^c - z_{pw,h} \}\!\} \|_{L^2(e)}^2 \leq C \sum_{j=1}^{2} h_{K_j}^5 \kappa^4 \|z\|_{L^\infty(K_j)}^2,$$

$$\| \{\!\{ \nabla_h(z_h^c - z_{pw,h}) \}\!\} \|_{L^2(e)}^2 \leq C \sum_{j=1}^{2} h_{K_j}^3 \kappa^4 \|z\|_{L^\infty(K_j)}^2.$$

Proof. Using the standard trace estimate

$$\| \{\!\{ z_h^c - z_{pw,h} \}\!\} \|_{L^2(e)}^2 \leq C \sum_{j=1}^{2} \left[\frac{1}{h_{K_j}} \|z_h^c - z_{pw,h}\|_{L^2(K_j)}^2 + h_{K_j} \|\nabla(z_h^c - z_{pw,h})\|_{L^2(K_j)}^2 \right].$$

Using the estimates for the basis functions in the previous lemma, on each triangle K_j,

$$\int_{K_j} |z_h^c - z_{pw,h}|^2 \, ds = \int_{K_j} \left| \sum_{\ell=1}^{3} z(\mathbf{a}_\ell^{K_j})(\lambda_\ell^K - \lambda_{pw,\ell}^K) \right|^2 \, ds \leq C h_{K_j}^6 \kappa^4 \|z\|_{L^\infty(K_j)}^2.$$

In the same way

$$\int_{K_j} |\nabla(z_h^c - z_{pw,h})|^2 \, ds = \int_{K_j} \left| \sum_{\ell=1}^{3} z(\mathbf{a}_\ell) \nabla(\lambda_\ell^{K_j} - \lambda_{pw,\ell}^{K_j}) \right|^2 \, ds \leq C h_{K_j}^4 \kappa^4 \|z\|_{L^\infty(K_j)}^2.$$

So

$$\| \{\!\{ z_h^c - z_{pw,h} \}\!\} \|_{L^2(e)}^2 \leq C \sum_{j=1}^{2} h_{K_j}^5 \kappa^4 \|z\|_{L^\infty(K_j)}.$$

Using the standard trace estimate again (noting that the basis functions are piecewise smooth)

$$\| \{\!\{\nabla_h(z_h^c - z_{pw,h})\}\!\} \|^2_{L^2(e)} \leq C \sum_{j=1}^{2} \left[\frac{1}{h_{K_j}} \|\nabla(z_h^c - z_{pw,h})\|^2_{L^2(K_j)} + h_{K_j} \|\nabla\nabla(z_h^c - z_{pw,h})\|^2_{L^2(K_j)} \right].$$

Using the estimates for the basis functions in the previous lemma and noting that since z_h^c is linear, $\nabla\nabla z_h^c = 0$,

$$\int_{K_j} |\nabla\nabla(z_h^c - z_{pw,h})|^2 \, dA = \int_{K_j} \left| \sum_{\ell=1}^{3} z(\mathbf{a}_\ell^{K_j})(\nabla\nabla\lambda_{h,\ell}^{K_j}) \right|^2 \leq C h_{K_j}^2 \kappa^4 \|z\|^2_{L^\infty(K_j)}.$$

So $\| \{\!\{\nabla_h(z_h^c - z_{pw,h})\}\!\} \|^2_{L^2(e)} \leq C \sum_{j=1}^{2} h_{K_j}^3 \kappa^4 \|z\|_{L^\infty(K_j)}$. This completes the proof. ∎

Now, since $z_{pw,h} \in V_h$, by the consistency of the PWDG scheme,

$$\int_\Omega (u - u_h)(\overline{u - u_h}) \, dA = A_h(u - u_h, z) = A_h(u - u_h, z - z_{pw,h}). \tag{5.1}$$

We first add and subtract the finite element piecewise linear interpolant on the mesh denoted z_h^c. This is not in the plane wave subspace V_h, so no terms simplify:

$$A_h(u - u_h, z - z_{pw,h}) = A_h(u - u_h, z - z_h^c) + A_h(u - u_h, z_h^c - z_{pw,h}). \tag{5.2}$$

We can now analyze the two terms on the right-hand side above. Using (3.6), the first term can be written

$$\begin{aligned}
&A_h(u - u_h, z - z_h^c) \\
&= \int_{\mathcal{E}_\mathcal{I}} [\![\nabla_h(u - u_h)]\!] \cdot \{\!\{\overline{z - z_h^c}\}\!\} \, ds - \int_{\mathcal{E}_\mathcal{I}} [\![(u - u_h)]\!] \cdot \{\!\{\nabla_h(\overline{z - z_h^c})\}\!\} \, ds \\
&\quad - \frac{1}{i\kappa} \int_{\mathcal{E}_\mathcal{I}} \beta \, [\![\nabla_h(u - u_h)]\!] \, [\![\nabla_h(\overline{z - z_h^c})]\!] \, ds + i\kappa \int_{\mathcal{E}_\mathcal{I}} \alpha \, [\![(u - u_h)]\!] \cdot [\![(\overline{z - z_h^c})]\!] \, ds \\
&\quad + \int_{\mathcal{E}_\mathcal{A}} (1 - \delta) \left[\frac{\partial(u - u_h)}{\partial \nu} + i\kappa(u - u_h) \right] (\overline{z - z_h^c}) \, ds \\
&\quad - \frac{1}{i\kappa} \int_{\mathcal{E}_\mathcal{A}} \delta \left[\frac{\partial(u - u_h)}{\partial \nu} + i\kappa(u - u_h) \right] \nabla_h(\overline{z - z_h^c}) \cdot \nu \, ds \\
&\quad + \int_{\mathcal{E}_\mathcal{D}} (u - u_h)(i\kappa\alpha(\overline{z - z_h^c}) - \nabla_h(\overline{z - z_h^c}) \cdot \nu) \, ds.
\end{aligned}$$

Note that $z = z_h^c = 0$ on $\mathcal{E}_\mathcal{D}$ and $[\![z - z_h^c]\!] = 0$ on $\mathcal{E}_\mathcal{I}$. In addition $u = 0$ on $\mathcal{E}_\mathcal{D}$, and u and its normal derivative are continuous across interior edges. Finally, u also satisfies the Dirichlet and impedance boundary conditions. So the above expression simplifies

as follows:

$$
\begin{aligned}
(5.3)\quad A_h(u-u_h, z-z_h^c) = &-\int_{\mathcal{E}_\mathcal{I}} [\![\nabla_h u_h]\!] \cdot \{\!\{\overline{z-z_h^c}\}\!\}\, ds + \int_{\mathcal{E}_\mathcal{I}} [\![u_h]\!] \cdot \{\!\{\nabla_h(\overline{z-z_h^c})\}\!\}\, ds \\
&+ \frac{1}{i\kappa}\int_{\mathcal{E}_\mathcal{I}} \beta\, [\![\nabla_h u_h]\!]\, [\![\nabla_h(\overline{z-z_h^c})]\!]\, ds \\
&+ \int_{\mathcal{E}_\mathcal{A}} (1-\delta)\left[g_A - \frac{\partial u_h}{\partial \nu} - i\kappa u_h\right](\overline{z-z_h^c})\, ds \\
&- \frac{1}{i\kappa}\int_{\mathcal{E}_\mathcal{A}} \delta\left[g_A - \frac{\partial u_h}{\partial \nu} - i\kappa u_h\right]\nabla_h(\overline{z-z_h^c})\cdot\nu\, ds \\
&+ \int_{\mathcal{E}_\mathcal{D}} u_h \nabla_h(\overline{z-z_h^c})\cdot\nu\, ds.
\end{aligned}
$$

Terms involving $z - z_h^c$ (nondifferentiated) can be estimated via the standard trace estimate. First,

$$
\begin{aligned}
&\left|-\int_{\mathcal{E}_\mathcal{I}} [\![\nabla_h u_h]\!]\cdot\{\!\{\overline{z-z_h^c}\}\!\}\, ds + \int_{\mathcal{E}_\mathcal{A}}(1-\delta)\left[g_A - \frac{\partial u_h}{\partial\nu} - i\kappa u_h\right](\overline{z-z_h^c})\, ds\right| \\
&\quad\le \sum_{e\in\mathcal{E}_\mathcal{I}} \kappa^{s-1/2}\|\beta^{1/2}\,[\![\nabla_h u_h]\!]\,\|_{L^2(e)}\kappa^{1/2-s}\|\beta^{-1/2}\,\{\!\{z-z_h^c\}\!\}\,\|_{L^2(e)} \\
&\qquad+\sum_{e\in\mathcal{E}_\mathcal{A}} \kappa^{s-1/2}\|(1-\delta)^{1/2}\left[g_A - \frac{\partial u_h}{\partial n} - i\kappa u_h\right]\|_{L^2(e)}\kappa^{1/2-s}\|(1-\delta)^{1/2}(z-z_h^c)\|_{L^2(e)}.
\end{aligned}
$$

Using the usual trace inequality (2.1), let e be an edge in the mesh shared by the elements K_1 and K_2, and then

$$
\begin{aligned}
\|\beta^{-1/2}\,\{\!\{z-z_h^c\}\!\}\,\|_{L^2(e)} &\le C\sum_{j=1}^{2}\left[\frac{1}{h_{K_j}^{1/2}}\|z-z_h^c\|_{L^2(K_j)} + h_{K_j}^{1/2}\|\nabla(z-z_h^c)\|_{L^2(K_j)}\right] \\
&\le C\sum_{j=1}^{2} h_{K_j}^{1+s}|z|_{H^{3/2+s}(K_j)},
\end{aligned}
$$

where we have also used standard error estimates for the piecewise linear interpolant.

The same estimate holds for the jump in $z - z_h^c$. Using the Cauchy–Schwarz inequality, we arrive at

$$
\begin{aligned}
&\left|-\int_{\mathcal{E}_\mathcal{I}} [\![\nabla_h u_h]\!]\cdot\{\!\{\overline{z-z_h^c}\}\!\}\, ds + \int_{\mathcal{E}_\mathcal{A}}(1-\delta)\left[g_A - \frac{\partial u_h}{\partial\nu} - i\kappa u_h\right](\overline{z-z_h^c})\, ds\right| \\
&\quad\le \Bigg[\kappa^{s-1/2}\|\beta^{1/2}h_e^{1+s}\,[\![\nabla_h u_h]\!]\,\|_{L^2(\mathcal{E}_\mathcal{I})} \\
&\qquad+\kappa^{s-1/2}\|(1-\delta)^{1/2}h_e^{1+s}\left[g_A - \frac{\partial u_h}{\partial n} - iku_h\right]\|_{L^2(\mathcal{E}_\mathcal{A})}\Bigg]\kappa^{1/2-s}|z|_{H^{3/2+s}(\Omega)}.
\end{aligned}
$$

Now we must perform the same estimate for terms in (5.3) involving derivatives of $z - z_h^c$:

$$\begin{aligned}
&\left| \int_{\mathcal{E}_\mathcal{I}} [\![u_h]\!] \{\!\{\nabla_h(\overline{z - z_h^c})\}\!\} \, ds - \frac{1}{i\kappa} \int_{\mathcal{E}_\mathcal{I}} \beta \, [\![\nabla_h u_h]\!] \, [\![\nabla_h(\overline{z - z_h^c})]\!] \, ds \right. \\
&\left. - \frac{\delta}{i\kappa} \int_{\mathcal{E}_\mathcal{A}} \left[g_A - \frac{\partial u_h}{\partial \nu} - ik u_h \right] \nabla_h(\overline{z - z_h^c}) \cdot \nu \, ds + \int_{\mathcal{E}_\mathcal{D}} u_h \nabla_h(\overline{z - z_h^c}) \cdot \nu \, ds \right| \\
&\quad \le \sum_{e \in \mathcal{E}_\mathcal{I}} \kappa^{s-1/2} \| \alpha^{1/2} [\![u_h]\!] \|_{L^2(e)} \kappa^{1/2-s} \| \alpha^{-1/2} \{\!\{\nabla_h(z - z_h^c)\}\!\} \|_{L^2(e)} \\
&\qquad + \sum_{e \in \mathcal{E}_\mathcal{I}} \kappa^{s-3/2} \| \beta^{1/2} [\![\nabla_h u_h]\!] \|_{L^2(e)} \kappa^{1/2-s} \| \beta^{1/2} [\![\nabla_h(z - z_h^c)]\!] \|_{L^2(e)} \\
&\qquad + \sum_{e \in \mathcal{E}_\mathcal{A}} \kappa^{s-3/2} \| \delta^{1/2} \left[g_A - \frac{\partial u_h}{\partial \nu} - i\kappa u_h \right] \|_{L^2(e)} \kappa^{1/2-s} \| \delta^{1/2} \frac{\partial (z - z_h^c)}{\partial \nu} \|_{L^2(e)} \\
&\qquad + \sum_{e \in \mathcal{E}_\mathcal{D}} \kappa^{s-1/2} \| \alpha^{1/2} u_h \|_{L^2(e)} \kappa^{1/2-s} \| \alpha^{-1/2} \nabla_h(z - z_h^c) \cdot \nu \|_{L^2(e)}.
\end{aligned}$$

We proceed as for the previous estimates. On an edge e between K_1 and K_2, we have, using the trace estimate (2.2),

$$\begin{aligned}
&\| \alpha^{-1/2} \{\!\{\nabla_h(z - z_h^c)\}\!\} \|_{L^2(e)} \\
&\qquad \le C \sum_{j=1}^{2} \left[\frac{1}{h_{K_j}^{1/2}} \| \nabla(z - z_h^c) \|_{L^2(K_j)} + h_{K_j}^s |\nabla(z - z_h^c)|_{H^{1/2+s}(K_j)} \right].
\end{aligned}$$

Since z_h^c is piecewise linear, $|\nabla(z - z_h^c)|_{H^{1/2+s}(K_j)} = |\nabla z|_{H^{1/2+s}(K_j)}$. Using usual estimates for the interpolant,

$$\| \alpha^{-1/2} \{\!\{\nabla_h(z - z_h^c)\}\!\} \|_{L^2(e)} \le C \sum_{j=1}^{2} h_{K_j}^s |z|_{H^{3/2+s}(K_j)}.$$

Other average and jump terms can be estimated in the same way. We arrive at

$$\begin{aligned}
&\left| \int_{\mathcal{E}_\mathcal{I}} [\![u_h]\!] \{\!\{\nabla_h(\overline{z - z_h^c})\}\!\} \, ds + \frac{1}{i\kappa} \int_{\mathcal{E}_\mathcal{I}} \beta \, [\![\nabla_h u_h]\!] \, [\![\nabla_h(\overline{z - z_h^c})]\!] \, ds \right. \\
&\left. - \frac{\delta}{i\kappa} \int_{\mathcal{E}_\mathcal{A}} \left[g_A - \frac{\partial u_h}{\partial \nu} - i\kappa u_h \right] \nabla_h(\overline{z - z_h^c}) \cdot \nu \, ds + \int_{\mathcal{E}_\mathcal{D}} u_h \nabla_h(\overline{z - z_h^c}) \cdot \nu \, ds \right| \\
&\quad \le C \Bigg[\kappa^{s-1/2} \| \alpha^{1/2} h_e^s [\![u_h]\!] \|_{L^2(\mathcal{E}_\mathcal{I})} + \kappa^{s-3/2} \| \beta^{1/2} h_e^s [\![\nabla_h u_h]\!] \|_{L^2(\mathcal{E}_\mathcal{I})} \\
&\qquad + \kappa^{s-3/2} \left\| \delta^{1/2} h_e^s \left[g_A - \frac{\partial u_h}{\partial \nu} - i\kappa u_h \right] \right\|_{L^2(\mathcal{E}_\mathcal{A})} \\
&\qquad + \kappa^{s-1/2} \| h_e^s \alpha^{1/2} u_h \|_{L^2(\mathcal{E}_\mathcal{D})} \Bigg] \kappa^{1/2-s} |z|_{H^{3/2+s}(\Omega)}.
\end{aligned}$$

We have thus proved the following lemmas.

LEMMA 5.4. *For h small enough, under the conditions on the mesh stated in section 2, there exists a constant C such that*

$$
\begin{aligned}
|A_h(u-u_h, z-z_h^c)| \le C \Big[& \kappa^{s-1/2} \|\beta^{1/2} h_e^{1+s} \left[\!\left[\nabla_h u_h \right]\!\right] \|_{L^2(\mathcal{E}_\mathcal{I})} \\
& + \kappa^{s-1/2} \|(1-\delta)^{1/2} h_e^{1+s} \left[g_A - \frac{\partial u_h}{\partial \nu} - i\kappa u_h \right] \|_{L^2(\mathcal{E}_\mathcal{A})} \\
& + \kappa^{s-1/2} \|\alpha^{1/2} h_e^s \left[\!\left[u_h \right]\!\right] \|_{L^2(\mathcal{E}_\mathcal{I})} + \kappa^{s-3/2} \|\beta^{1/2} h_e^s \left[\!\left[\nabla_h u_h \right]\!\right] \|_{L^2(\mathcal{E}_\mathcal{I})} \\
& + \kappa^{s-3/2} \|\delta^{1/2} h_e^s \left[g_A - \frac{\partial u_h}{\partial \nu} - i\kappa u_h \right] \|_{L^2(\mathcal{E}_\mathcal{A})} \\
& + \kappa^{s-1/2} \|h_e^s \alpha^{1/2} u_h\|_{L^2(\mathcal{E}_\mathcal{D})} \Big] \kappa^{1/2-s} |z|_{H^{3/2+s}(\Omega)}.
\end{aligned}
$$

Here, C is independent of the mesh, the solution, and κ.

It remains to estimate $A_h(u-u_h, z_h^c - z_{pw,h})$. Recall that $z_{pw,h}$ is defined element by element according to Lemma 5.3 and

$$
\begin{aligned}
& A_h(u-u_h, z_h^c - z_{pw,h}) \\
& \quad = -\int_{\mathcal{E}_\mathcal{I}} \left[\!\left[\nabla_h u_h \right]\!\right] \cdot \left\{\!\!\left\{ \overline{z_h^c - z_{pw,h}} \right\}\!\!\right\} \, ds + \int_{\mathcal{E}_\mathcal{I}} \left[\!\left[u_h \right]\!\right] \left\{\!\!\left\{ \nabla_h (\overline{z_h^c - z_{pw,h}}) \right\}\!\!\right\} \, ds \\
& \qquad + \frac{1}{i\kappa} \int_{\mathcal{E}_\mathcal{I}} \beta \left[\!\left[\nabla_h u_h \right]\!\right] \left[\!\left[\nabla_h (\overline{z_h^c - z_{pw,h}}) \right]\!\right] \, ds - i\kappa \int_{\mathcal{E}_\mathcal{I}} \alpha \left[\!\left[u_h \right]\!\right] \left[\!\left[(\overline{z_h^c - z_{pw,h}}) \right]\!\right] \, ds \\
& \qquad + \int_{\mathcal{E}_\mathcal{A}} (1-\delta) \left[g_A - \frac{\partial u_h}{\partial \nu} - i\kappa u_h \right] (\overline{z_h^c - z_{pw,h}}) \, ds \\
& \qquad - \frac{\delta}{i\kappa} \int_{\mathcal{E}_\mathcal{A}} \left[g_A - \frac{\partial u_h}{\partial \nu} - i\kappa u_h \right] \nabla_h (\overline{z_h^c - z_{pw,h}}) \cdot \nu \, ds \\
& \qquad - \int_{\mathcal{E}_\mathcal{D}} u_h (i\kappa\alpha (\overline{z_h^c - z_{pw,h}}) - \nabla_h (\overline{z_h^c - z_{pw,h}}) \cdot \nu) \, ds.
\end{aligned}
$$

As before, considering an edge e between elements K_1 and K_2 and using the fact that β is constant,

$$
\begin{aligned}
& \left| \int_e \left\{\!\!\left\{ \overline{z_h^c - z_{pw,h}} \right\}\!\!\right\} \cdot \left[\!\left[\nabla_h (u-u_h) \right]\!\right] \, ds \right| \\
& \quad \le \|\beta^{1/2} h_e^{3/2} \left[\!\left[\nabla_h u_h \right]\!\right] \|_{L^2(e)} \|\beta^{-1/2} h_e^{-3/2} \left\{\!\!\left\{ z_h^c - z_{pw,h} \right\}\!\!\right\} \|_{L^2(e)} \\
& \quad \le C \|\beta^{1/2} h_e^{3/2} \left[\!\left[\nabla_h u_h \right]\!\right] \|_{L^2(e)} \sqrt{\sum_{j=1}^2 h_e^{-3} h_{K_j}^5 \kappa^4 \|z\|^2_{L^\infty(K_j)}} \\
& \quad \le C\kappa^2 \|\beta^{1/2} h_e^{3/2} \left[\!\left[\nabla_h u_h \right]\!\right] \|_{L^2(e)} \sqrt{\sum_{j=1}^2 h_{K_j}^2 \|z\|^2_{L^\infty(K_j)}} \\
& \quad \le C \left[\frac{1}{2\epsilon} \|\beta^{1/2} h_e^{3/2} \left[\!\left[\nabla_h u_h \right]\!\right] \|^2_{L^2(e)} + \frac{\epsilon}{2} \kappa^4 \sum_{j=1}^2 h_{K_j}^2 \|z\|^2_{L^\infty(K_j)} \right]
\end{aligned}
$$

for any constant $\epsilon > 0$.

Now adding over all edges in $\mathcal{E}_{\mathcal{I}}$,

$$\left| \int_{\mathcal{E}_{\mathcal{I}}} \{\!\{ \overline{z_h^c - z_{pw,h}} \}\!\} \cdot [\![\nabla_h (u - u_h)]\!] \, ds \right|$$

$$\leq C \left[\frac{1}{2\epsilon} \| \beta^{1/2} h_e^{3/2} [\![\nabla_h u_h]\!] \|^2_{L^2(\mathcal{E}_{\mathcal{I}})} + \frac{\epsilon}{2} \mathrm{area}(\Omega) \kappa^4 \|z\|^2_{L^\infty(\Omega)} \right].$$

Similarly, using again Lemma 5.3,

$$\left| \int_{\mathcal{E}_{\mathcal{I}}} [\![u_h]\!] \{\!\{ \nabla_h (\overline{z_h^c - z_{pw,h}}) \}\!\} \, ds \right|$$

$$\leq \| \alpha^{1/2} h_e^{1/2} [\![u_h]\!] \|_{L^2(e)} \| \alpha^{-1/2} h_e^{-1/2} \{\!\{ \nabla_h (z_h^c - z_{pw,h}) \}\!\} \|_{L^2(e)}$$

$$\leq C \left[\frac{1}{2\epsilon} \| h_e^{1/2} \alpha^{1/2} [\![u_h]\!] \|^2_{L^2(e)} + \frac{\epsilon}{2} \kappa^4 \sum_{j=1}^{2} h_{K_j}^2 \|z\|^2_{L^\infty(K_j)} \right].$$

Proceeding as above, we can estimate each of the terms in the expansion of A_h and prove the following estimate.

LEMMA 5.5. *Under the assumptions on the mesh in section* 2, *there is a constant* C *independent of* h, κ, u, *and* u_h *such that*

$$|A_h(u - u_h, z_h^c - z_{pw,h})|$$

$$\leq C \Bigg\{ \frac{1}{2\epsilon} \Bigg[\| \beta^{1/2} h_e^{3/2} [\![\nabla_h u_h]\!] \|^2_{L^2(\mathcal{E}_{\mathcal{I}})} + \kappa^2 \| \alpha^{1/2} h_e^{3/2} [\![u_h]\!] \|^2_{L^2(\mathcal{E}_{\mathcal{I}})}$$

$$+ \left\| (1-\delta)^{1/2} h_e^{3/2} \left[g_A - \frac{\partial u_h}{\partial \nu} - i\kappa u_h \right] \right\|^2_{L^2(\mathcal{E}_{\mathcal{A}})}$$

$$+ \| \alpha^{1/2} h_e^{1/2} [\![u_h]\!] \|^2_{L^2(\mathcal{E}_{\mathcal{I}})} + \kappa^{-2} \| \beta^{1/2} h_e^{1/2} [\![\nabla_h u_h]\!] \|^2_{L^2(\mathcal{E}_{\mathcal{I}})}$$

$$+ \kappa^{-2} \left\| \delta^{1/2} h_e^{1/2} \left[g_A - \frac{\partial u_h}{\partial \nu} - i\kappa u_h \right] \right\|^2_{L^2(\mathcal{E}_{\mathcal{A}})} \Bigg] + \frac{\epsilon}{2} \kappa^4 \mathit{area}(\Omega) \|z\|^2_{L^\infty(\Omega)} \Bigg\}.$$

Since $s \leq 1/2$ and using the estimates for $\|z\|_{H^{3/2+s}(\Omega)}$ from section 4, we obtain the following.

THEOREM 5.6. *Under the assumptions on the mesh in section* 2, *for any sufficiently fine mesh there is a constant* C *independent of* h, d_Ω, u, *and* u_h *such that*

$$\|u - u_h\|_{L^2(\Omega)} \leq C \eta(u_h),$$

where

$$\begin{aligned}\eta(u_h)^2 = \Bigg\{ & \kappa^{2s-1}(d_\Omega\kappa)^{1-2s}(1+d_\Omega\kappa)^2)\Bigg[\|\beta^{1/2}h_e^{1+s}\,[\![\nabla_h u_h]\!]\,\|^2_{L^2(\mathcal{E}_\mathcal{I})} \\ & + \left\|(1-\delta)^{1/2}h_e^{1+s}\left[g_A - \frac{\partial u_h}{\partial \nu} - i\kappa u_h\right]\right\|^2_{L^2(\mathcal{E}_\mathcal{A})} \\ & + \|\alpha^{1/2}h_e^s\,[\![u_h]\!]\,\|^2_{L^2(\mathcal{E}_\mathcal{I})} + \kappa^{-2}\|\beta^{1/2}h_e^s\,[\![\nabla_h u_h]\!]\,\|^2_{L^2(\mathcal{E}_\mathcal{I})} \\ & + \kappa^{-2}\left\|\delta^{1/2}h_e^s\left[g_A - \frac{\partial u_h}{\partial \nu} - i\kappa u_h\right]\right\|^2_{L^2(\mathcal{E}_\mathcal{A})} \|h_e^s\alpha^{1/2}u_h\|^2_{L^2(\mathcal{E}_\mathcal{D})}\Bigg] \\ & + (\kappa d_\Omega)^2(1+d_\Omega^4\kappa^4)\Bigg[\|\beta^{1/2}h_e^{3/2}\,[\![\nabla_h u_h]\!]\,\|^2_{L^2(\mathcal{E}_\mathcal{I})} + \kappa^2\|\alpha^{1/2}h_e^{3/2}\,[\![u_h]\!]\,\|^2_{L^2(\mathcal{E}_\mathcal{I})} \\ & + \left\|(1-\delta)^{1/2}h_e^{3/2}\left[g_A - \frac{\partial u_h}{\partial \nu} - i\kappa u_h\right]\right\|^2_{L^2(\mathcal{E}_\mathcal{A})} \\ & + \|\alpha^{1/2}h_e^{1/2}\,[\![u_h]\!]\,\|^2_{L^2(\mathcal{E}_\mathcal{I})} + \kappa^{-2}\|\beta^{1/2}h_e^{1/2}\,[\![\nabla_h u_h]\!]\,\|^2_{L^2(\mathcal{E}_\mathcal{I})} \\ & + \kappa^{-2}\left\|\delta^{1/2}h_e^{1/2}\left[g_A - \frac{\partial u_h}{\partial \nu} - i\kappa u_h\right]\right\|^2_{L^2(\mathcal{E}_\mathcal{A})}\Bigg]\Bigg\}.\end{aligned}$$

Remark 3. The right-hand side is now a new a posteriori error indicator for PWDG. Note there is no longer an overall factor of $h^{-1/2}$ compared to the estimate in Theorem 4.1. On a refined mesh at fixed κ dropping the higher order terms in mesh size, a reasonable choice of indicator is $\tilde{\eta}$ defined by

$$\begin{aligned}\tilde{\eta}(u_h)^2 = \kappa^{2s-1}(d_\Omega\kappa)^{1-2s}(1+d_\Omega\kappa)^2)\Bigg[& \|\alpha^{1/2}h_e^s\,[\![u_h]\!]\,\|^2_{L^2(\mathcal{E}_\mathcal{I})} + \kappa^{-2}\|\beta^{1/2}h_e^s\,[\![\nabla_h u_h]\!]\,\|^2_{L^2(\mathcal{E}_\mathcal{I})} \\ & + \kappa^{-2}\left\|\delta^{1/2}h_e^s\left[g_A - \frac{\partial u_h}{\partial \nu} - i\kappa u_h\right]\right\|^2_{L^2(\mathcal{E}_\mathcal{A})} \\ & + \|h_e^s\alpha^{1/2}u_h\|^2_{L^2(\mathcal{E}_\mathcal{D})}\Bigg].\end{aligned}$$

In practice, we shall find the choice $s = 0$ gives a reliable but pessimistic indicator.

Proof. Using (4.5) and Lemma 5.4, for any $\epsilon_1 > 0$ there are constants C_1 and C_2 such that

$$\begin{aligned}& |A_h(u-u_h, z-z_h^c)| \\ & \quad \le \frac{C_1\kappa^{2s-1}}{\epsilon_1}\Bigg[\|\beta^{1/2}h_e^{1+s}\,[\![\nabla_h u_h]\!]\,\|_{L^2(\mathcal{E}_\mathcal{I})} \\ & \qquad + \left\|(1-\delta)^{1/2}h_e^{1+s}\left[g_A - \frac{\partial u_h}{\partial \nu} - i\kappa u_h\right]\right\|_{L^2(\mathcal{E}_\mathcal{A})} \\ & \qquad + \|\alpha^{1/2}h_e^s\,[\![u_h]\!]\,\|_{L^2(\mathcal{E}_\mathcal{I})} + \kappa^{-1}\|\beta^{1/2}h_e^s\,[\![\nabla_h u_h]\!]\,\|_{L^2(\mathcal{E}_\mathcal{I})} \\ & \qquad + \kappa^{-1}\left\|\delta^{1/2}h_e^s\left[g_A - \frac{\partial u_h}{\partial \nu} - i\kappa u_h\right]\right\|_{L^2(\mathcal{E}_\mathcal{A})} + \|h_e^s\alpha^{1/2}u_h\|_{L^2(\mathcal{E}_\mathcal{D})}\Bigg]^2 \\ & \quad + C_2\epsilon_1(d_\Omega\kappa)^{1-2s}(1+d_\Omega\kappa)^2\|u-u_h\|^2_{L^2(\Omega)}.\end{aligned}$$

Using (4.6) and Lemma 5.5, for any $\epsilon > 0$ there are constant C_3 and C_4 such that

$$\begin{aligned}
&|A_h(u-u_h, z_h^c - z_{pw,h})| \\
&\quad \le \frac{C_3}{\epsilon}\Bigg[\|\beta^{1/2} h_e^{3/2} [\![\nabla_h u_h]\!] \|^2_{L^2(\mathcal{E}_\mathcal{I})} + \kappa^2 \|\alpha^{1/2} h_e^{3/2} [\![u_h]\!] \|^2_{L^2(\mathcal{E}_\mathcal{I})} \\
&\qquad + \left\| (1-\delta)^{1/2} h_e^{3/2} \left[g_A - \frac{\partial u_h}{\partial \nu} - i\kappa u_h \right] \right\|^2_{L^2(\mathcal{E}_\mathcal{A})} \\
&\qquad + \|\alpha^{1/2} h_e^{1/2} [\![u_h]\!] \|^2_{L^2(\mathcal{E}_\mathcal{I})} + \kappa^{-2} \|\beta^{1/2} h_e^{1/2} [\![\nabla_h u_h]\!] \|^2_{L^2(\mathcal{E}_\mathcal{I})} \\
&\qquad + \kappa^{-2} \left\| \delta^{1/2} h_e^{1/2} \left[g_A - \frac{\partial u_h}{\partial \nu} - i\kappa u_h \right] \right\|^2_{L^2(\mathcal{E}_\mathcal{A})} \Bigg] \\
&\qquad + C_4 \epsilon (\kappa d_\Omega)^2 (1 + d_\Omega^4 \kappa^4) \|u - u_h\|^2_{L^2(\Omega)}.
\end{aligned}$$

Choosing $\epsilon_1 (C_2 (d_\Omega \kappa)^{1-2s} (1 + d_\Omega \kappa)^2) = 1/4$ and ϵ such that $C_4 \epsilon (\kappa d_\Omega)^2 (1 + d_\Omega^4 \kappa^4) = 1/4$ and using (5.1) and (5.2), we obtain that, for an overall constant C,

$$\begin{aligned}
&\|u - u_h\|^2_{L^2(\Omega)} \\
&\le C \Bigg\{ \kappa^{2s-1} (d_\Omega \kappa)^{1-2s} (1 + d_\Omega \kappa)^2) \Bigg[\|\beta^{1/2} h_e^{1+s} [\![\nabla_h u_h]\!] \|^2_{L^2(\mathcal{E}_\mathcal{I})} \\
&\quad + \left\| (1-\delta)^{1/2} h_e^{1+s} \left[g_A - \frac{\partial u_h}{\partial \nu} - i\kappa u_h \right] \right\|^2_{L^2(\mathcal{E}_\mathcal{A})} \\
&\qquad + \|\alpha^{1/2} h_e^s [\![u_h]\!] \|^2_{L^2(\mathcal{E}_\mathcal{I})} + \kappa^{-2} \|\beta^{1/2} h_e^s [\![\nabla_h u_h]\!] \|^2_{L^2(\mathcal{E}_\mathcal{I})} \\
&\qquad + \kappa^{-2} \left\| \delta^{1/2} h_e^s \left[g_A - \frac{\partial u_h}{\partial \nu} - i\kappa u_h \right] \right\|^2_{L^2(\mathcal{E}_\mathcal{A})} \\
&\qquad + \|h_e^s \alpha^{1/2} u_h\|^2_{L^2(\mathcal{E}_\mathcal{D})} \Bigg] \\
&\quad + (\kappa d_\Omega)^2 (1 + d_\Omega^4 \kappa^4) \Bigg[\|\beta^{1/2} h_e^{3/2} [\![\nabla_h u_h]\!] \|^2_{L^2(\mathcal{E}_\mathcal{I})} + \kappa^2 \|\alpha^{1/2} h_e^{3/2} [\![u_h]\!] \|^2_{L^2(\mathcal{E}_\mathcal{I})} \\
&\qquad + \left\| (1-\delta)^{1/2} h_e^{3/2} \left[g_A - \frac{\partial u_h}{\partial \nu} - i\kappa u_h \right] \right\|^2_{L^2(\mathcal{E}_\mathcal{A})} \\
&\qquad + \|\alpha^{1/2} h_e^{1/2} [\![u_h]\!] \|^2_{L^2(\mathcal{E}_\mathcal{I})} + \kappa^{-2} \|\beta^{1/2} h_e^{1/2} [\![\nabla_h u_h]\!] \|^2_{L^2(\mathcal{E}_\mathcal{I})} \\
&\qquad + \kappa^{-2} \left\| \delta^{1/2} h_e^{1/2} \left[g_A - \frac{\partial u_h}{\partial \nu} - i\kappa u_h \right] \right\|^2_{L^2(\mathcal{E}_\mathcal{A})} \Bigg] \Bigg\}. \qquad \square
\end{aligned}$$

6. Numerical results. We now test the new residual estimators derived in the previous section using the UWVF choice of parameters $\alpha = \beta = \delta = 1/2$. In the following numerical tests, we iteratively apply the classical refinement sequence

$$\text{SOLVE} - \text{ESTIMATE} - \text{MARK} - \text{REFINE}.$$

In the ESTIMATE phase of the following experiments, we rank the effective contributions to the right-hand side of the a posteriori bound given in Theorem 5.6

from the element K using a proxy for the residual formula

$$\eta_K^2 = \|\alpha^{1/2} h_e^s [\![u_h]\!] \|_{L^2(\partial K)}^2 + \frac{1}{\kappa^2}\|\beta^{1/2} h_e^s [\![\nabla_h u_h]\!] \|_{L^2(\partial K)}^2 + \frac{1}{\kappa^2}\|\delta^{1/2} h_e^s \left[g_A - \frac{\partial u_h}{\partial \nu} - i\kappa u_h \right] \|_{L^2(\partial K)}^2 + \|\alpha^{1/2} h_e^s u_h\|_{L^2(\partial K)}^2.$$

Following Dörfler [6], the elements responsible for the top θ fraction of $\eta := \sum_K \eta_K$ are marked for refinement in the MARK phase. In the REFINE phase, we use a recursive longest edge bisection [20] to produce a new mesh with guaranteed lower bounds for the smallest element angles. The recursive longest edge bisection algorithm is chosen because it propagates the refinement beyond the elements marked in the MARK phase to achieve this goal.

6.1. Smooth solutions on an L-shaped domain. We start with several results for the regular Bessel function solution considered in section 4 and defined by equation (4.10) so that $\kappa = 12$. Since we are on the L-shaped domain, we choose $s = 1/6$. These results are shown in Figure 5 and can be compared to the results in Figures 3 and 4. Although the efficiency shown in the right-hand column for each choice of p_K still deteriorates for the L^2 norm as the mesh is refined, the rate of rise is less compared to the previous indicator. In addition, the efficiency of the indicator improves for larger p_K.

6.2. A singular solution. We now consider a physically relevant solution with an appropriate singularity at the reentrant corner. We choose the exact solution of (1.1) given by

$$u(\mathbf{x}) = J_\xi(\kappa r)\sin(\xi\theta)$$

for $\xi = 2/3$ and $\kappa = 12$. In this case, near $r = 0$, $u \approx Cr^{2/3}\sin(2\theta/3)$ so $u \in H^{5/3-\epsilon}(\Omega)$ for any $\epsilon > 0$ and we again take $s = 1/6$ in the estimators. The boundary conditions (only Dirichlet in our numerical experiments) are determined from this exact solution.

The computed solution and the corresponding final mesh after 12 refinement steps is shown in Figure 6 (starting from the mesh in Figure 2). Clearly, the algorithm has refined the mesh near the reentrant corner as expected.

Results for $p_K = 3$ and $p_K = 4$ are shown in Figure 7. In this case, we start with a mesh obtained by two steps of uniform refinement of the mesh in Figure 2. This is because for low p_K, the original initial mesh is too coarse to produce any approximation of the solution. If we start with the mesh in Figure 2, the algorithm does correctly refine uniformly, but many adaptive steps are needed before accuracy starts to improve. The results show that our indicator works even when $p_K = 3$, even though piecewise linear polynomials cannot be well approximated in the sense of Lemma 5.1. Note that the fact that the curve for η falls below the actual error in Figure 7 does not indicate that we have lost reliability. We have scaled the η so that the error on the coarsest mesh and scaled η agree. (See the discussion for Figure 3.) A reliable indicator would follow the error curve but because of our arbitrary scaling could be above or below the actual error.

Results for $p_K = 5, 7, 9$ are shown in Figure 8, starting with the mesh in Figure 2 and using $s = 1/6$ in our estimator. Convergence is slower than for the smooth solution, but the efficiency of the indicators is improved although it does deteriorate as the mesh is refined. In Figure 8, we also show an estimate of the condition number of the matrix corresponding to the PWDG discretization computed using the `condest`

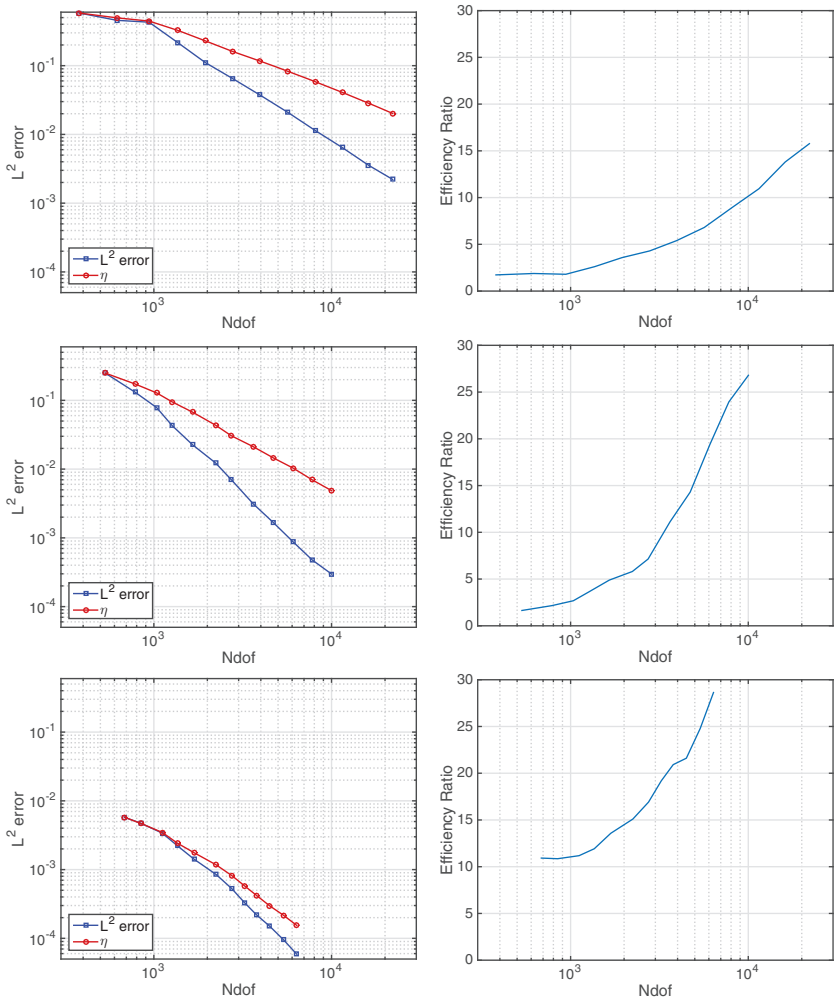

FIG. 5. *Results for the smooth Bessel function solution on the L-shaped domain using* $s = 1/6$. *The top row is for* $p_K = 5$, *the middle for* $p_K = 7$, *and the bottom for* $p_K = 9$. *The left column shows the indicator (normalized to the actual error at the start) and relative* L^2 *error as a function of the number of degrees of freedom. The right column measures the efficiency of the indicator and shows the ratio of the true error in the* L^2*norm to the residual. Ideally, this curve should be flat (at least for a well resolved solution).*

function of MATLAB. This example, with strong local refinement near the reentrant corner, shows particularly poor conditioning.

Clearly, since we are keeping the number of directions fixed per element, the condition blows up sharply as we refine the mesh. Ultimately, this will cause the discrete problem to be too ill-conditioned to solve. Note, however, that we are not interested in the coefficients of the plane waves in the solution, but the solution values themselves. These are obtained by summing the local plane wave contributions, and this may help explain why the results remain more stable than might be expected from the vast condition numbers encountered. However, an error analysis to support this suggestion is currently lacking.

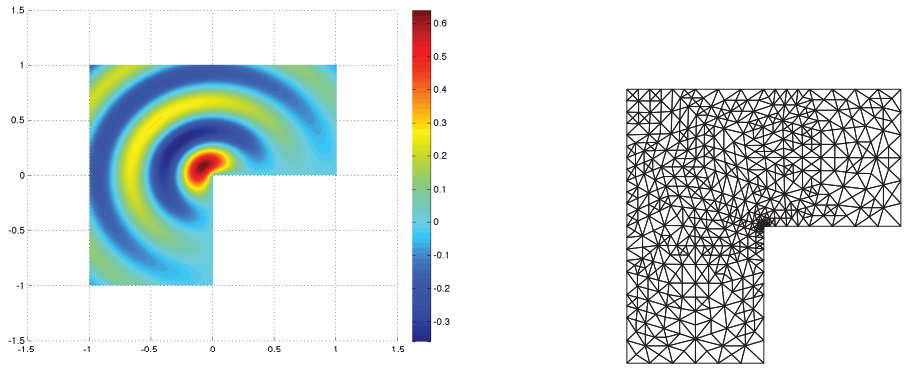

(a) Computed Solution (b) Refined Mesh

FIG. 6. *The numerical solution and final mesh after* 12 *iterations when* $\xi = 2/3$ *(singular solution) and* $\kappa = 12$ *using* $p_K = 7$ *plane waves per element. At the resolution of the graphics, the exact and computed solution are indistinguishable.*

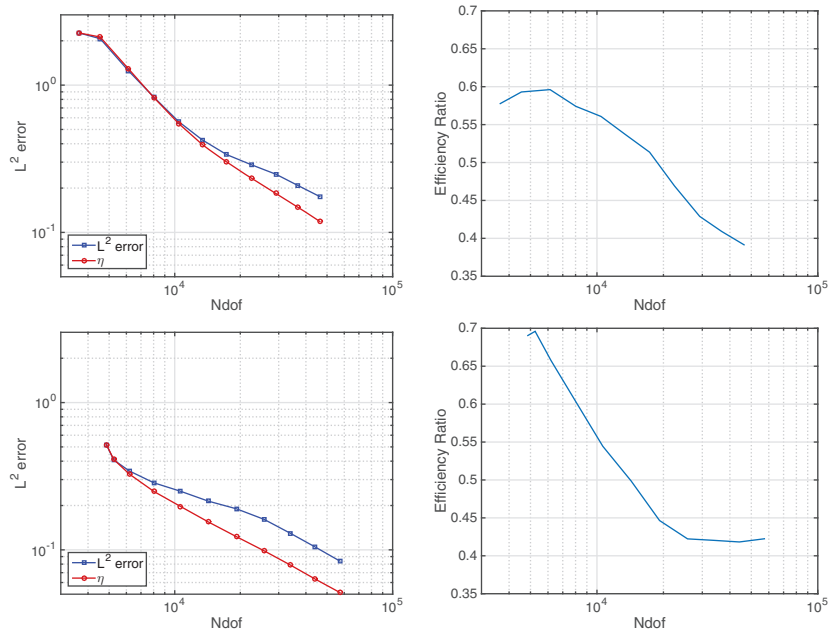

FIG. 7. *Results for the singular solution (Bessel function with* $\xi = 2/3$*) using* $p_K = 3$ *(top row) and* $p_K = 4$ *(bottom row) starting from two levels of refinement of the initial grid in Figure* 2*. This figure has the same columns as Figure* 5*. As expected, there is little difference between the convergence rate for the two methods (the a priori error estimates are the same order for* $p_K = 3$ *and* $p_K = 4$*), but the residual estimator behaves better in the case when* $p_K = 4$ *in that the efficiency curve flattens out.*

6.3. Internal reflection. For the Helmholtz equation, besides the standard elliptic corner singularities mentioned above, adaptivity may also help deal with boundary layers that can arise at interfaces between regions with different refractive indices. We now consider adaptivity for the transmission and reflection of a plane wave across a fluid-fluid interface on a square domain $\Omega := (-1, 1)^2$ with two different refractive

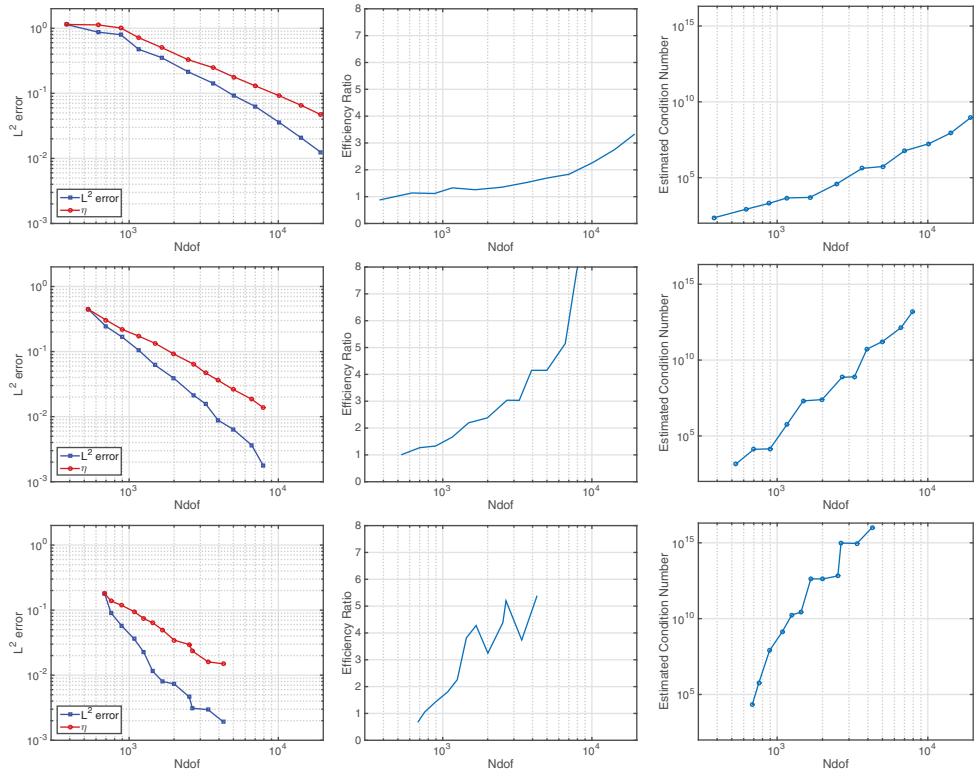

FIG. 8. *Results for the singular solution (Bessel function with $\xi = 2/3$) using $p_K = 5$ (top row), $p_K = 7$ (middle row), and $p_K = 9$ (bottom row). We start from the initial grid in Figure 2. This figure has the same layout as in Figure 5 except that the third column shows the estimated condition number of the system matrix as a function of the number of degrees of freedom.*

indices. The interface is located at $y = 0$. The problem now is to find $u \in H^1(\Omega)$ such that

$$\Delta u + \kappa^2 \epsilon_r u = 0 \text{ in } \Omega \tag{6.1}$$

subject to appropriate boundary conditions, where

$$\epsilon_r(x, y) = \begin{cases} n_1^2 & \text{if } y < 0, \\ n_2^2 & \text{if } y > 0. \end{cases}$$

We choose $n_1 = 2$ and $n_2 = 1$. Then it is easy to show that for any angle $0 \le \theta_i < \pi/2$ and $\mathbf{d} = (\cos(\theta_i), \sin(\theta_i))$, the following is a solution of (6.1):

$$u(x, y) = \begin{cases} T \exp(i(K_1 x + K_2 y)) & \text{if } y > 0, \\ \exp(i\kappa n_1(d_1 x + d_2 y)) + R \exp(i\kappa n_1(d_1 x - d_2 y)) & \text{if } y < 0, \end{cases}$$

where $K_1 = \kappa n_1 d_1$ and $K_2 = \kappa\sqrt{n_2^2 - n_1^2 d_1^2}$ and

$$R = -(K_2 - \kappa n_1 d_2)/(K_2 + \kappa n_1 d_2),$$
$$T = 1 + R.$$

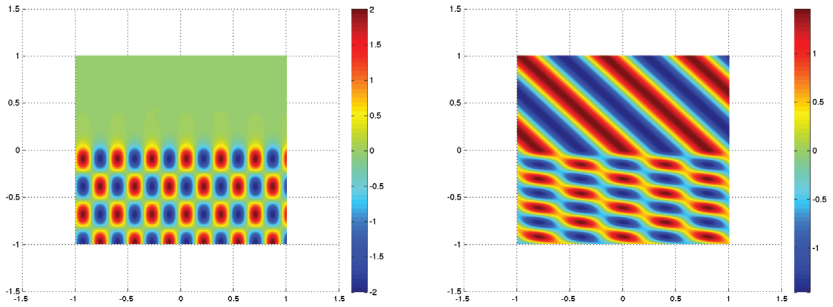

(a) $\theta_{inc} = 29°, \theta_i < \theta_{crit}$ (b) $\theta_{inc} = 69°, \theta_i > \theta_{crit}$

FIG. 9. *Numerical solutions after* 12 *iterations when* $k = 11$ *and* $n_1 = 2$, $n_2 = 1$, $p_K = 7$ *plane waves per element. When* $\theta_i < \theta_{crit}$, *the wave decays exponentially into the upper half of the plane as shown for* $\theta_i = 29°$ *(left panel). When* $\theta_i = 69°$, *the wave is transmitted into the upper half of the square (right panel).*

If $n_2^2 - n_1^2 d_1^2 < 0$ (i.e., if $n_2 > n_1$ and d_1 is large enough), then K_2 is imaginary (we choose a positive imaginary part) and the solution for $y > 0$ decays exponentially into the upper half plane. (Physically, this is said to be total internal reflection since the wave above the interface is vanishingly low amplitude far from the interface.) If d_1 is small enough (i.e., close to normal incidence), the wave is refracted at the interface and a traveling wave is seen above and below the interface. Thus, there is a critical angle $\theta_i = \theta_{crit}$ such that for $\theta_i > \theta_{crit}$ the wave is refracted, and for $\theta_i < \theta_{crit}$ we have internal reflection. This is shown in Figure 9. The case of internal reflection is challenging for a plane wave based method since evanescent (or exponentially decaying) waves are not in the basis. We therefore investigate if our residual estimators can appropriately refine the mesh in this case. (This not a problem covered by our theory.)

In particular we use Dirichlet boundary conditions derived from the exact solution (assuming κ^2 is not an interior eigenvalue for the domain) and choose the wavenumber $\kappa = 11$. In view of the fact that the domain is convex with a smooth interface, we choose $s = 1/2$ in the estimator.

Representative meshes produced by our algorithm are shown in Figure 10. Starting with the initial mesh in panel (a), we generate the mesh in panel (b) when $\theta_i = 69°$. The algorithm correctly refines the lower half square more, and there is an abrupt transition to the less refined upper half. In panel (c), we show the mesh when $\theta = 29°$. In this case, the algorithm correctly does not refine well above the interface, but at the interface $y = 0$ some refinement occurs even for $y > 0$ in order to resolve the exponentially decaying solutions there. We shall only consider the case $\theta_i = 29°$ (internal reflection) from now on.

Detailed error plots when $p_K = 5, 7, 9$ are shown in Figure 11. The results are broadly similar to our previous results. The error is decreased by the refinement strategy, but efficiency generally deteriorates as the mesh is refined. Again, the error indicator for the higher order method, $p_K = 9$, is best.

For our final results, we return to the L-shaped domain and $p_K = 9$. We have seen that the efficiency of the indicator deteriorates as the mesh is refined when we take $s = 1/6$ in the residual indicators. We have also seen that the maximum choice of s is $s = 1/2$, and we now test the indicator for $s = 1/2$ for the smooth and singular Bessel function solutions. Results are shown in Figure 12. The efficiency in the L^2 norm is improved but still deteriorates as the mesh is refined.

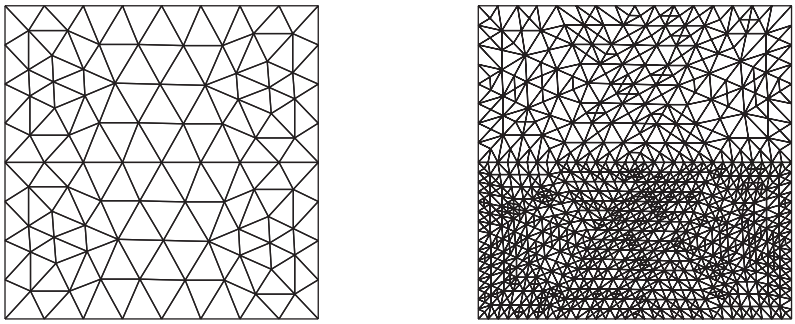

(a) Initial Mesh (b) $\theta_{inc} = 69°$

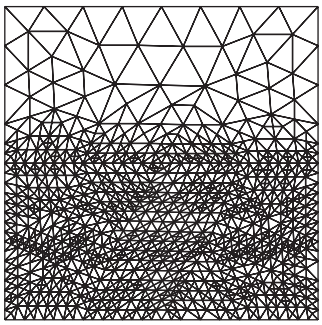

(c) $\theta_{inc} = 29°$

FIG. 10. *Initial mesh and the meshes after* 12 *adaptive iterations for transmission* ($\theta_i = 69°$) *and internal reflection* ($\theta_i = 29°$). *Here,* $p_K = 7$.

6.4. Bessel function basis. At the suggestion of an anonymous referee, we have also tried a local Bessel function basis. In [17], it is shown computationally that, provided the basis is scaled appropriately, such a basis results in a lower condition number for the UWVF on a uniform mesh compared to the same number of equally spaced plane waves. Since we are using constant weights in this section, we hope that the scaling used in [17] will also provide enhanced conditioning here. In particular, as in [17], we use

$$u_h|_K = \sum_{m=-\mu_K}^{\mu_K} u_m^K \frac{J_m(\kappa|\mathbf{x} - \mathbf{c}_K|)}{\kappa\sqrt{(J_m'(\kappa h_K))^2 + (J_m(\kappa h_K))^2}} \exp(im\theta),$$

where $\mathbf{c}_K$ is the centroid of triangle K and $\{u_m^K\}_{m=-\mu_K}^{\mu_K}$ are expansion coefficients. The local mesh size h_K is chosen here for convenience to be the average distance of the centroid from the three vertices of K. Results are shown in Figure 13, which should be compared to Figure 8. (In both cases, $s = 1/6$.) On the one hand, the error and efficiency plots in the left and center column of Figure 13 are very similar to graphs in the left and center columns of Figure 8. This is unsurprising given the close relationship between plane wave and Bessel function bases (see, for example, [10]). On the other hand, the scaled Bessel basis gives significantly better conditioning than the plane wave based scheme.

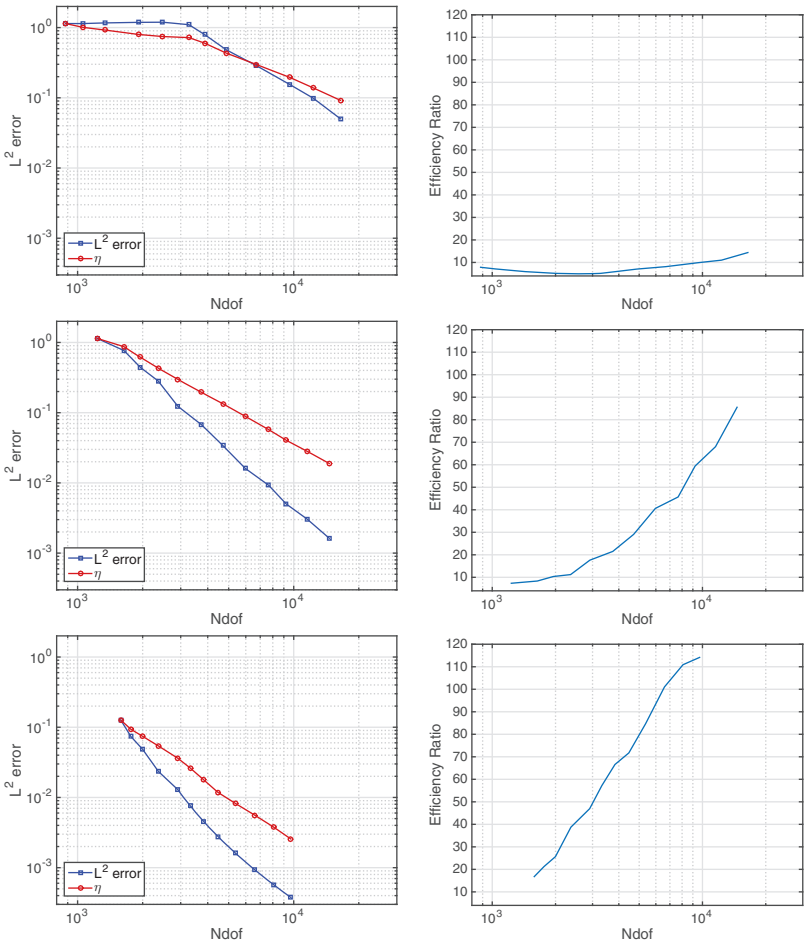

FIG. 11. *Results for total internal reflection when* $p_K = 5$ *(top row),* $p_K = 7$ *(middle row), and* $p_K = 9$ *(bottom row). Here, we choose* $s = 1/2$*. This figure has the same layout as Figure* 5.

7. Conclusion. We have derived two new a posteriori error indicators for the PWDG method. One is based on existing theory, and the second is based on the observation that plane wave basis functions can approximate piecewise linear finite elements on a fine mesh. Using the usual Doerfler marking strategy, the estimators drive mesh adaptivity that gives convergence for a smooth solution as well as coping with singularities and evanescent modes. The indicators give apparently reliable estimates for the L^2 norm, but even for the improved indicators, the efficiency tends to deteriorate as the mesh is refined. The condition number of the matrix for the PWDG rises rapidly as the mesh size decreases. Limited testing suggests that using a Bessel function basis gives significantly better conditioning behavior.

The indicators have a parameter s that depends on the solution domain. A safe choice is $s = 0$, but better efficiency is obtained by taking larger s, and numerically $s = 1/2$ appears to be a good choice.

Usually, error is estimated in the energy norm, and we will investigate a posteriori error indicators for the broken H^1 norm in a future publication.

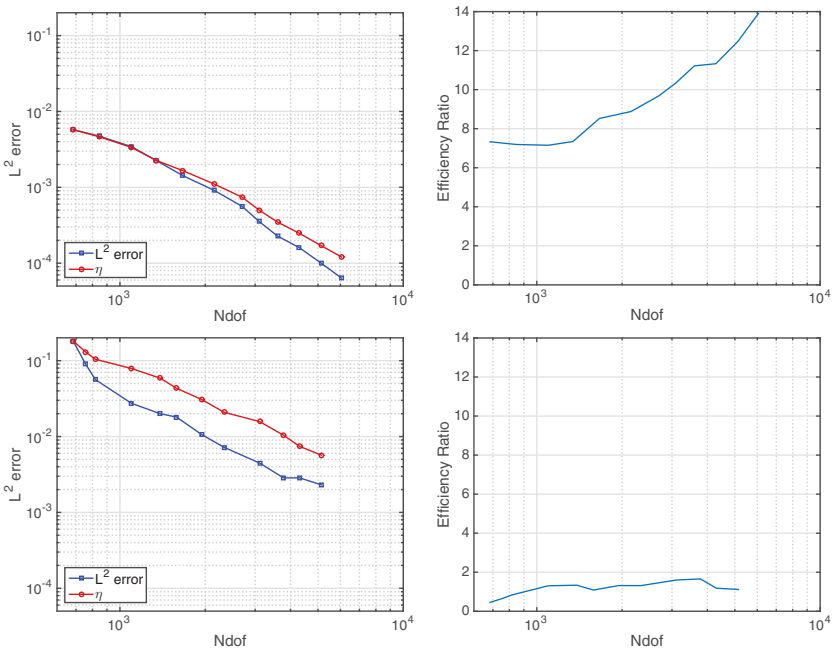

FIG. 12. *Results for $p_K = 9$ and $s = 1/2$ on the L-shape domain. Top: smooth solution. Bottom: singular solution. The columns of this figure have the same layout as Figure* 5.

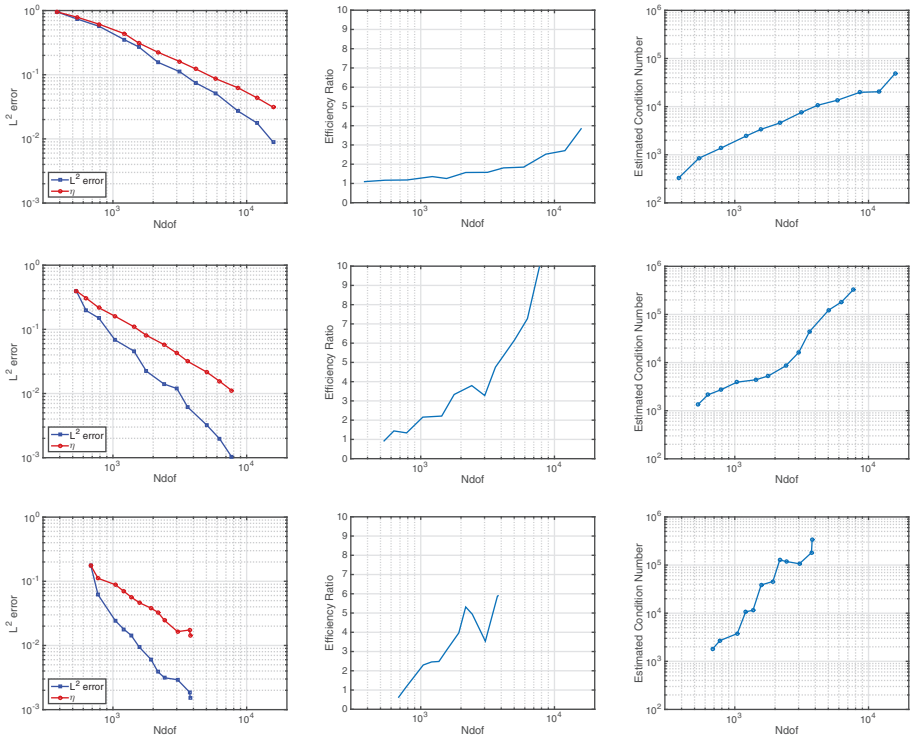

FIG. 13. *Results for the singular solution (Bessel function with $\xi = 2/3$) using local Bessel functions $\mu_K = 2$ (top row), $\mu_K = 3$ (middle row), and $\mu_K = 4$ (bottom row). We start from the initial grid in Figure 2. This figure has the same layout as Figure 8.*

REFERENCES

[1] M. Amara, S. Chaudhry, J. Diaz, R. Djellouli, and S.L. Fiedler, *A local wave tracking strategy for efficiently solving mid- and high-frequency Helmholtz problems*, Comput. Methods Appl. Mech. Engrg., 276 (2014), pp. 473–508.

[2] T. Betcke and J. Phillips, *Approximation by Dominant Wave Directions in Plane Wave Methods*, preprint, http://discovery.ucl.ac.uk/1342769/.

[3] A. Buffa and P. Monk, *Error estimates for the Ultra Weak Variational Formulation of the Helmholtz equation*, ESAIM Math. Model. Numer. Anal., 42 (2008), pp. 925–940.

[4] O. Cessenat, *Application d'une Nouvelle Formulation Variationnelle aux Équations D'ondes Harmoniques. Problèmes de Helmholtz* $2D$ *et de Maxwell* $3D$, Ph.D. thesis, Université Paris IX Dauphine, Paris, 1996.

[5] O. Cessenat and B. Després, *Application of an ultra weak variational formulation of elliptic PDEs to the two-dimensional Helmholtz problem*, SIAM J. Numer. Anal., 35 (1998), pp. 255–299.

[6] W. Dörfler, *A convergent adaptive algorithm for Poisson's equation*, SIAM J. Numer. Anal., 33 (1996), pp. 1106–1124.

[7] S. Esterhazy and J.M. Melenk, *On stability of discretizations of the Helmholtz equation*, in Numerical Analysis of Multiscale Problems, I.G. Graham, T.Y. Hou, O. Lakkis, and R. Scheichl, eds., Lect. Notes Comput. Sci. Eng. 83, Springer, Heidelberg, 2012, pp. 285–324.

[8] E. Giladi and J. Keller, *A hybrid numerical asymptotic method for scattering problems*, J. Comput. Phys., 174 (2001), pp. 226–247.

[9] C.J. Gittelson and R. Hiptmair, *Dispersion analysis of plane wave discontinuous Galerkin methods*, Internat. J. Numer. Methods Engrg., 98 (2014), pp. 313–323.

[10] C. Gittelson, R. Hiptmair, and I. Perugia, *Plane wave discontinuous Galerkin methods*, ESAIM Math. Model. Numer. Anal., 43 (2009), pp. 297–331.

[11] R. Hiptmair, A. Moiola, and I. Perugia, *Plane wave discontinuous Galerkin methods for the* $2D$ *Helmholtz equation: Analysis of the p-version*, SIAM J. Numer. Anal., 49 (2011), pp. 264–284.

[12] R. Hiptmair, A. Moiola, and I. Perugia, *Error analysis of Trefftz-discontinuous Galerkin methods for the time-harmonic Maxwell equations*, Math. Comp., 82 (2013), pp. 247–268.

[13] R. Hiptmair, A. Moiola, and I. Perugia, *Plane wave discontinuous Galerkin methods: Exponential convergence of the hp-version*, Found. Comput. Math., 2015, DOI:10.1007/s10208-015-9260-1.

[14] R. Hiptmair, A. Moiola, and I. Perugia, *Trefftz discontinuous Galerkin methods for acoustic scattering on locally refined meshes*, Appl. Numer. Math., 79 (2014), pp. 79–91.

[15] T. Huttunen, M. Malinen, and P.B. Monk, *Solving Maxwell's equations using the Ultra Weak Variational Formulation*, J. Comput. Phys., 223 (2007), pp. 731–758.

[16] T. Luostari, T. Huttunen, and P. Monk, *Error estimates for the ultra weak variational formulation in linear elasticity*, ESAIM Math. Model. Numer. Anal., 47 (2013), pp. 183–211.

[17] T. Luostari, T. Huttunen, and P. Monk, *Improvements for the ultra weak variational formulation*, Internat. J. Numer. Methods Engrg., 94 (2013), pp. 598–624.

[18] T. Luostari, T. Huttunen, and P. Monk, *The ultra weak variational formulation of thin clamped plates*, J. Comput. Phys., 260 (2014), pp. 85–106.

[19] J. Melenk, A. Parsania, and S. Sauter, *General DG-methods for highly indefinite Helmholtz problems*, J. Sci. Comput., 57 (2013), pp. 1–46.

[20] W.F. Mitchell, *A comparison of adaptive refinement techniques for elliptic problems*, ACM Trans. Math. Software, 15 (1989), pp. 326–347.